Circulation Research

ORIGINAL RESEARCH

Endothelial NOX1 Drives Obesity via Skeletal Muscle Mitochondrial Dysfunction

Kai Huang,* Yuanli Huang,* Yuhan Zhang, Yixuan Zhang, Nicholas W. Hatch, Julie K. Freed, Hua Cai

BACKGROUND: Presently, we investigated hypothesized roles and mechanisms of cell type–specific, selective activation of different vascular NOX (NADPH oxidase) isoforms in obesity and metabolic syndrome.

METHODS: Wild-type, NOX1/2/4 global knockout mice, endothelial/VSMC-specific NOX1 knockout mice, or vascular endothelial-speicifc NOX1 knockin mice were exposed to high-fat diet feeding prior to phenotypical analyses of obesity and metabolic syndrome, as well as of exercise capacity, skeletal muscle mitochondrial function, and novel genetic signatures.

RESULTS: Expression of NOX1 was significantly upregulated in wild-type mice fed a high-fat diet. Global knockout of NOX1 (NOX1$^{-/y}$), rather than of NOX2/NOX4, markedly abrogated high-fat feeding–induced body weight/fat mass gain, preadipocyte differentiation, fatty liver, glucose intolerance, and insulin/leptin resistance. Intriguingly, endothelial-specific NOX1 knockout (Cdh5cre [cadherin 5 (vascular endothelial cadherin) promoter–driven Cre recombinase (endothelial-specific Cre expression)]-NOX1CKO), rather than vascular smooth muscle-specific NOX1 knockout (Myh11cre [myosin heavy chain 11 promoter–driven Cre recombinase (smooth muscle–specific Cre expression)]-NOX1CKO), substantially alleviated obesity and metabolic syndrome. Consistently, endothelial-specific NOX1 knockin mice (Cdh5cre-NOX1CKI) fed a high-fat diet displayed exaggerated metabolic disorders. Endothelial cell–specific knockout/knockin of NOX1 was confirmed using endothelial cell washout experiments. Food/water intakes were not different from corresponding controls in high-fat fed NOX1$^{-/y}$, Cdh5cre-NOX1CKO, or Cdh5cre-NOX1CKI mice, indicating no difference in energy intake. Instead, spontaneous activity, exercise capacity, mitochondrial oxygen consumption/ATP production, skeletal muscle mitochondrial function (ROS production and swelling activity), and mitochondrial cristae structure were all substantially improved in NOX1$^{-/y}$ or Cdh5cre-NOX1CKO mice, indicating augmented energy expenditure attributed to preserved skeletal muscle mitochondrial function. Supportively, Cdh5cre-NOX1CKI mice displayed deteriorated exercise capacity and skeletal muscle mitochondrial dysfunction. Endothelium-dependent vasorelaxation was restored in high-fat fed NOX1$^{-/y}$ or Cdh5cre-NOX1CKO mice, confirming improved endothelial function. RNA-sequencing identified 4 genes (*Cntnap4* [contactin-associated protein-like 4], *Sgsm1*, *Tll2*, and *Syt9*) and 7 genes (*Odf3l2*, *Col9a1* [collagen type IX alpha 1 chain], *Cldn23*, *Atp5g2*, *Nkx6-3*, *Ntsr2*, and *Zfp69*) significantly downregulated/upregulated in high-fat fed Cdh5cre-NOX1CKO mice, among which Cntnap4 and Col9a1 linked to muscular disorders. Importantly, we observed marked upregulation of NOX1 in isolated coronary arteries from human patients with obesity.

CONCLUSIONS: Taken together, our data for the first time establish a novel and paradigm-shifting concept that endothelial NOX1 drives systematic metabolic phenotypes, via impairment in skeletal muscle mitochondrial dysfunction with novel genetic signatures. Tissue-specific targeting of endothelial NOX1 and novel candidate genes may prove to be robustly effective in treating obesity and metabolic syndrome.

GRAPHIC ABSTRACT: A graphic abstract is available for this article.

Key Words: metabolic syndrome ■ mitochondrial diseases ■ muscle, skeletal ■ NADPH oxidases ■ obesity ■ reactive oxygen species

Meet the First Author, see p e000756 | Editorial, see Article by Craige

Correspondence to: Hua Cai, MD, PhD, Department of Anesthesiology and Perioperative Medicine, Department of Medicine, David Geffen School of Medicine, University of California, 650 Charles E Young Dr, Los Angeles, Los Angeles, CA 90095. Email hcai@mednet.ucla.edu
*K. Huang and Y. Huang contributed equally.
Supplemental Material is available at https://www.ahajournals.org/doi/suppl/10.1161/CIRCRESAHA.125.326768.

Circulation Research is available at www.ahajournals.org/journal/res

Novelty and Significance

What Is Known?

- Oxidative stress is involved in the development of obesity and metabolic syndrome.
- Activation of NOX (NADPH oxidase) has been implicated in obesity and metabolic syndrome.

What New Information Does This Article Contribute?

- NOX1 (NOX isoform 1), but not NOX2 (NOX isoform 2) or NOX4 (NOX isoform 4), mediates the development of obesity and metabolic syndrome.
- Endothelial-specific activation of NOX1 drives obesity and metabolic syndrome attributed to exercise incapacity and reduced energy expenditure.
- Endothelial-specific NOX1 activation mediates skeletal muscle mitochondrial dysfunction to result in deficiencies in exercise capacity and energy expenditure.
- Novel genetic signatures of skeletal Cntnap4 (contactin-associated protein-like 4) and Col9a1 (collagen type IX alpha 1 chain) have been identified as potential new targets for the treatment of obesity and metabolic syndrome.
- Our findings for the first time mechanistically demonstrate a critical driving role of endothelial NOX1 activation in the development of obesity and metabolic syndrome.

Oxidative stress attributed to activation of NOX has been implicated in obesity and metabolic syndrome. However, this study reveals a novel role of endothelial-specific activation of NOX1 in driving these conditions by impairing exercise capacity to reduce energy expenditure, while NOX2 and NOX4 are dispensable. Mechanistically, endothelial NOX1 activation induces skeletal muscle mitochondrial dysfunction, leading to metabolic deficiencies. In addition, novel genetic signatures, Cntnap4 and Col9a1, were identified as potential therapeutic targets. These findings provide the first mechanistic evidence that endothelial NOX1 is a key driver of obesity and metabolic syndrome, offering new insights for targeted interventions.

Nonstandard Abbreviations and Acronyms

BMI	body mass index
Cdh5cre	cadherin 5 (vascular endothelial cadherin) promoter–driven Cre recombinase (endothelial-specific Cre expression)
Cntnap4	contactin-associated protein-like 4
Col9a1	collagen type IX alpha 1 chain
DHFR	dihydrofolate reductase
EC	endothelial cell
eNOS	endothelial nitric oxide synthase
IPA	Ingenuity Pathway Analysis
Myh11cre	myosin heavy chain 11 promoter–driven Cre recombinase (smooth muscle–specific Cre expression)
NOX	NADPH oxidase
NOX1	NOX isoform 1
NOX1CKI	cre-inducible NOX1$^{flox/flox}$ knockin/floxed mice
NOX1CKO	cre-inducible NOX1$^{flox/flox}$ knockout/floxed mice
NOX2	NOX isoform 2
NOX3	NOX isoform 3
NOX4	NOX isoform 4
PCR	polymerase chain reaction
RCR	respiratory control ratio
ROS	reactive oxygen species
UCLA	University of California, Los Angeles
WT	wild type

Obesity has proven to be a global epidemic with, however, unclear molecular mechanisms for its development and progression.[1] It is estimated that 39% to 49% of the population worldwide (2.8–3.5 billion people) is overweight or obese.[1,2] Obesity is a chronic, complex, heterogeneous disease that impacts all organ systems, resulting in severe health consequences and a huge economic burden for patients and society.[3,4] WHO estimates that at least 2.8 million people die each year as a result of being obese or overweight.[5] Although pharmacological, surgical, and device interventions have been used to treat obesity, these practices have not been consistently effective in managing obesity and its complications at the population level.[4,6,7] Currently, there are 6 major Food and Drug Administration–approved antiobesity medications: phentermine, orlistat, phentermine/topiramate extended release, lorcaserin, naltrexone sustained release/bupropion sustained release, and liraglutide.[3] Nonetheless, all of these drugs have varying degrees of adverse effects or contraindications and are not optimal for long-term treatment of obesity.[3] Therefore, identification of detailed molecular mechanisms of obesity is in urgent need to enable development of novel and effective therapeutics for the treatment of obesity and metabolic syndrome.

Oxidative stress has been implicated in the development of obesity and metabolic syndrome.[8,9] We have previously established an innovative, paradigm-shifting concept that vascular oxidative stress is a driving force for the development of systematic obesity and metabolic syndrome, rather than being a mere consequence.[8] Mice with overproduction of reactive oxygen species (ROS) in the vasculature displayed markedly exaggerated obesity

and metabolic syndrome in response to high-fat feeding.[8] p22^{phox} (also known as cytochrome b-245 light chain), as the only membrane-bound subunit for NOX (NADPH oxidase), is required for catalytic activation of NOX1 (NOX isoform 1), NOX2 (NOX isoform 2), NOX3 (NOX isoform 3), and NOX4 (NOX isoform 4),[10,11] among which NOX1, NOX2, and NOX4 are expressed in the vascular cells.[12,13] Of note, NOX family enzymes have emerged as the predominant sources of ROS production during the pathogenesis of cardiovascular diseases.[11,14–18] We and others have identified differential roles of different NOX isoforms in mediating the development of different pathological conditions of hypertension, aortic aneurysms, diabetic vascular dysfunction under either type 1 or type 2 conditions, ischemia-reperfusion injury of the heart, and cardiac arrhythmia.[11,19–30] Therefore, we sought to identify whether there is a direct, causal role of NOX in driving obesity and metabolic syndrome in response to high-fat feeding, the specific isoform(s) of NOX that is(are) involved, potential tissue/cell-specific roles of NOX isoforms, and the underlying molecular mechanisms.

In this study, our data clearly demonstrate that global knockout of NOX1, rather than of NOX2 or NOX4, protects against obesity and metabolic syndrome under high-fat feeding. NOX1 expression was markedly upregulated in wild-type (WT) mice fed a high-fat diet. Endothelial cell (EC) NOX1, rather than vascular smooth muscle NOX1, is specifically involved in this process. While energy intake was not different, high-fat feeding–induced impairment in energy expenditure, spontaneous activity, exercise capacity, mitochondrial oxygen consumption/ATP production, skeletal muscle mitochondrial function, and mitochondrial cristae structure were all substantially improved in global or endothelial-specific NOX1 knockout mice, whereas these phenotypes and mechanistic alternations were exaggerated in endothelial-specific NOX1 knockin mice. The endothelial-specific knockout/knockin of NOX1 was validated using EC washout experiments. Therefore, enhanced energy expenditure attributed to improved skeletal muscle mitochondrial function results in restored spontaneous activity and exercise capacity, which underlies protection against obesity and metabolic syndrome by global or endothelial-specific deletion of NOX1. Endothelium-dependent vasorelaxation was restored in high-fat–fed NOX1$^{-/y}$ or Cdh5cre (cadherin 5 [vascular endothelial cadherin] promoter–driven Cre recombinase [endothelial-specific Cre expression])-cre-inducible NOX1$^{flox/flox}$ knockout (Cdh5cre-NOX1CKO), confirming improved endothelial function. Novel targets of *Cntnap4* (contactin-associated protein-like 4) and *Col9a1* (collagen type IX alpha 1 chain) were identified by RNA-sequencing and validation analyses in Cdh5cre-NOX1CKO mice to account for the mechanistic regulations of skeletal muscle function. Importantly, we observed marked upregulation of NOX1 in the coronary arteries of human patients with obesity. For the first time, these findings establish a novel, significant, specific, and selective role of endothelial NOX1 in driving obesity and metabolic syndrome via impairment in skeletal muscle mitochondrial function/energy expenditure with novel genetic signatures, targeting of which may be robustly effective in treating human metabolic disorders.

METHODS

Data Availability

The original data supporting the main findings of this study are available from the corresponding author upon reasonable request. Except for the most critical methods paragraphs presented below, other detailed methods have been included in the Supplemental Material.

Generation of Endothelial Specific NOX1CKO and NOX1 CKI mice and Experimental Design

The NOX1 floxed mice were generated by the Transgenic Mouse Facility at the University of California, Irvine, using the European Conditional Mouse Mutagenesis Program–targeted male embryonic stem cells cell line. In brief, a loxP (locus of X-over P1 sites recognized by Cre recombinase) NOX1 targeting construct with simultaneous insertion of an orphan loxP site and an FRT-neo-FRT (Flippase recognition target [FRT]-flanked neomycin resistance cassette)-loxP resistance cassette was inserted into the NOX1 genomic locus to target exon 3 to exon 8 (E3–E8) of NOX1 by Cre-mediated excision. For genotyping of NOX1 floxed mice the polymerase chain reaction (PCR) primers used were 5′- GTACTAAACAGAGAAAGGCTCT CCC-3′, 5′-TACTGGGACAGCTTCCTGCATCCC-3′, and 5′-CAACGGGTTCTTCTGTTAGTCC-3′. The PCR amplification was performed using the conditions of 95°C for 3 minutes, followed by 35 cycles of 92°C for 30 s, 61°C for 30 s, and 72°C for 30 s. PCR products were separated on 1.8% agarose gel, with a 407-base pair band indicating the presence of the mutant allele. A 527-base pair product from PCR indicates the WT allele. The mice were backcrossed in-house to the C57BL/6 background for >10 generations.

The floxed mice used to generate endothelial-specific NOX1 knockin mice were created in-house. A floxed stop codon was inserted before the genomic locus of the *NOX1* gene that can be excised once Cre is induced by tamoxifen. For the NOX1CKI genotyping, the PCR primers used were 5′-CTCAAGCTTCGAATATGGGAAACTG-3′ and 5′-GATCCAATGGCTTTCTCAGTGTACG-3′. The PCR amplification was performed using the conditions of 95°C for 5 minutes, followed by 29 cycles of 92°C for 30 s, 56°C for 30 s, and 72°C for 30 s. PCR products were separated on 1.8% agarose gel, with a 290-base pair band indicating the presence of a transgenic band. The mice were backcrossed in-house to the C57BL/6 background for >10 generations.

The Cdh5 (cadherin 5; PAC [P1 artificial chromosome])-CreERT2 (Cre recombinase–estrogen receptor T2 fusion protein [tamoxifen-inducible Cre recombinase]) founder mice (endothelial Cre mice)[31] were generously provided by Dr Ralf Adams from the Vascular Development Laboratory, Cancer

Research UK London Research Institute, London, United Kingdom. For Cdh5 (PAC)-CreERT2 genotyping, PCR primers used were 5′-GCCTGCATTACCGGTCGATGCAACGAGTG-3′ and 5′-CTGGCAATTTCGGCTATACGTAACAGGGTG-3′. The PCR amplification was performed using the conditions of 95 °C for 5 minutes, followed by 29 cycles of 92 °C for 30 s, 60 °C for 30 s, and 72 °C for 30 s. PCR products were separated on 1.8% agarose gel, with a 345-base pair band indicating the presence of a transgenic band. The tg(Myh11-cre/ERT2)1Soff (vascular smooth muscle cells [VSMC] Cre) was originally purchased from Jackson Laboratory (Stock No: 019079). For Myh11-cre/ERT2 genotyping, PCR primers used were 5′-TGA CCC CAT CTC TTC ACT CC-3′ and 5′-AGT CCC TCACAT CCT CAGGTT-3′. The PCR amplification was performed using the conditions of 94 °C for 2 minutes, followed by 10 cycles of 94 °C for 20 s, 65 °C for 15 s, and 68 °C for 15 s, and then followed by 28 cycles of 94 °C for 15 s, 60 °C for 15 s, and 72 °C for 15 s. PCR products were separated on 1.8% agarose gel, with a 287-base pair band indicating the presence of a transgenic band. The NOX1 floxed mice were crossed with Cdh5-cre or Myh11-cre to generate Cdh5cre-NOX1CKO (EC-specific NOX1 knockout mice) or Myh11cre (myosin heavy chain 11 promoter–driven Cre recombinase [smooth muscle–specific Cre expression])-NOX1CKO (VSMC-specific NOX1 knockout mice) for experiments. The inducible NOX1$^{flox/flox}$ knockin/floxed mice were crossed with Cdh5-cre mice to generate Cdh5cre-NOX1CKI (EC-specific NOX1 knockin/overexpressing) mice for experiments. All of the mice have been bred and maintained at the University of California, Los Angeles (UCLA). Tamoxifen was dissolved in a sunflower seed oil/ethanol (10:1) mixture at 10 mg/mL, and 5-week-old Cdh5cre-NOX1CKO/WT, Myh11cre-NOX1CKO/WT, and Cdh5cre-NOX1CKI/WT mice were injected with 2 mg of tamoxifen intraperitoneally for 5 consecutive days.[8,32,33]

Animal Studies Using WT and Various Knockout and Knockin Mice

All animals mentioned above and experimental procedures were approved by the institutional animal care and use committee at UCLA. Before experimentation, animals were kept in ventilated cages with free access to water and standard chow and cared for by Division of Laboratory Animal Medicine staff until 8 weeks old. Mice were randomly divided into 2 dietary groups and fed either regular chow (5053, 13.2% fat; LabDiet, St. Louis, MO) or a high-fat diet (with 42% calories from fat, TD.88137, Envigo, New Jersey, NY) for 8 weeks.

Measurements of Food and Water Intake, and Determination of Oxygen Consumption in Individual Animals Using Metabolic Cages

Diet and water intake of mice were monitored weekly for 8 consecutive weeks until the end of the protocol. Oxygen consumption was measured using an Oxymax Comprehensive Lab Animal Monitoring System (Oxymax-CLAMS; Columbus Instruments, Columbus, OH). Eight weeks after the mice were fed a regular diet or a high-fat diet, the animals were subjected to Metabolic Cage analyses. Animals were individually housed in an open-circuit chamber for 3 days with ad libitum access to food and water. Oxygen consumption was measured by the Oxymax system for mice housed individually, and the data were analyzed using the CLAMS Examination Tool (CLAX; Columbus Instruments), version 2.1.0.[34]

Assessment of Spontaneous Activity

After 8 weeks of dietary intervention (regular chow versus high-fat diet), mouse spontaneous activity in the 12-hour dark cycle was monitored by video-recording using infrared webcams, and the real-time motions of the individual animals were analyzed using motion-detection software as we previously published.[8]

Assessment of Exercise Capacity

As mentioned above, mice were randomly assigned to either a regular chow or a high-fat diet group and fed accordingly for 8 weeks before subsequent experiments. Mouse exercise capacity was examined using a specialized mouse Treadmill (Exer 3/6 model, Columbus Instruments) as previously described with modifications.[35] Before measurement, mice were trained for 2 days at a constant speed of 6 m/min for 30 minutes. For assessment of exercise capacity, mice were subjected to a 5-minute warm-up period at 6 m/min, after which treadmill speed was incrementally increased to 30 m/min, and the mice were run for 40 minutes with speed escalating at 1.2 m/min every 2 minutes. An electric shock at 1.0-mA current was applied at the back of the treadmill to motivate mice to run. Exhaustion was defined as the point when mice remained on shockers for >10 s and were not able to jump back on the track. Exercise capacity was evaluated by time, total distance traveled, and speed at exhaustion point.

Mitochondrial Isolation and Assessment of Respirational Capacity

Upon harvesting of tissues, mitochondria were freshly isolated by differential centrifugation. In brief, freshly harvested skeletal muscles were homogenized using a DWK Life Sciences Kimble Kontes Duall Tissue Grinders (size 23, Kimble, Thermo-Fisher Scientific, Grand Island, NY) in homogenization buffer containing 250-mmol/L sucrose, 1-mmol/L ethylene glycol-bis (β-aminoethyl ether)-N, N, N′, N′-tetraacetic acid, 10-mmol/L HEPES, and 10-mmol/L Tris-HCl, pH 7.4. The homogenates were centrifuged at 800*g* for 7 minutes, and then, the supernatants were transferred to new tubes and centrifuged at 4000*g* for 15 minutes. The pellet was rinsed with homogenization buffer without ethylene glycol-bis (β-aminoethyl ether)-N, N, N′, N′-tetraacetic acid and then centrifuged at 4000*g* for 15 minutes. Rinsed pellets were resuspended in homogenization buffer without ethylene glycol-bis (β-aminoethyl ether)-N, N, N′, N′-tetraacetic acid. Respirational capacity of fresh mitochondria was examined using a Seahorse XF 24-3 analyzer (Seahorse Bioscience, UCLA Biosciences Cellular Bioenergetics Core) according to the manufacturer's instructions. The respiratory control ratio (RCR) was calculated as State III/State IVo, induced by the addition of Oligomycin.

Mitochondrial Swelling Assay

Freshly isolated mitochondria were incubated with swelling buffer containing 250-mmol/L sucrose, 10-mmol/L Tris (pH 7.4), and 5-mmol/L succinate for 1 minute at room temperature

before swelling was initiated by the addition of 250-μmol/L $CaCl_2$. Mitochondrial swelling was measured by monitoring the decrease in absorbance at 540 nm using a Synergy Plate Reader (Synergy H1 Hybrid Reader, Biotek/Agilent, Santa Clara, CA) as we previously described.[8,27]

Examination of Mitochondrial Cristae Structures by Electron Microscopy

Freshly harvested soleus muscle was immediately immersed in electron microscopy grade fixing solution (0.1M PB with 2.5% glutaraldehyde and 4% paraformaldehyde, pH 7.4). Specimen processing and imaging were performed at the UCLA Brain Research Institute Electron Microscopy Core Laboratory. Muscular mitochondria were imaged by JEOL 100CX transmission electron microscope (JEOL Ltd) at magnifications of ×2900 and ×7200, respectively.

RNA-Sequencing/RNA-Sequencing Analysis

RNAs isolated from soleus muscles of experimental mice (3 each group from 4 experimental groups of Cdh5cre-WT mice under regular diet, Cdh5cre-WT mice under high-fat diet, Cdh5cre-NOX1CKO mice under regular diet, and Cdh5cre-NOX1CKO mice under high-fat diet) were subjected to RNA-sequencing at the UCLA Technology Center for Genomics & Bioinformatics. KAPA Stranded RNA-SeqKit was used for preparing the libraries for RNA-sequencing. Sequencing was performed on an Illumina HiSeq 3000 for a single read, 50 runs. Data quality checks were done on Illumina SAV. Demultiplexing was performed by using Illumina Bcl2fastq2, version 2.17, program. Reads were first mapped to the latest UCSC transcript set with Bowtie2, version 2.1.0, and gene expression levels were estimated by RSEM, version 1.2.15. Gene expression was normalized by the trimmed mean of M-values. The edgeR program was used to identify the differentially expressed genes. RNA species that increase >2-fold or decrease >2-fold in the soleus muscle of WT mice under high-fat feeding (group 3) compared with WT mice with a regular diet (group 1) were screened out. Then, protein-coding RNAs were chosen from these RNA species. The protein-coding RNAs decreased by >1.5-fold or increased by >1.5-fold in Cdh5Cre-NOX1CKO mice under high-fat feeding (group 4) compared with WT littermates under high-fat feeding (group 3) were selected. The significantly upregulated or downregulated protein-coding RNAs ($P<0.05$) were further analyzed by Ingenuity Pathway Analysis (IPA; see below) to explore their relationship to skeletal muscle function.

IPA Analysis

The differentially regulated protein-coding RNAs identified by RNA-sequencing analysis were analyzed by QIAGEN IPA (content version: 68752261, https://www.qiagenbioinformatics.com/products/ingenuity-pathway-analysis) to reveal those implicated in skeletal and muscular disorders for subsequent analyses.

Analysis of NOX1 Expression in Human Patients

Coronary artery samples of a total of 15 human subjects (body mass index [BMI] <25, n=6; BMI >25, n=9) were used for the determination of NOX1 expression. All protocols were approved by the institutional review board at the Medical College of Wisconsin to collect fresh, otherwise discarded, explanted, donated hearts from the Versiti Institute. Specimens from individuals were categorized based on BMI. Coronary arteries were dissected and immediately transferred to ice-cold PBS solution to preserve tissue integrity. Connective tissue was carefully removed, and the arteries were divided into sections. Sections of the coronary arteries were lysated and subjected to WB analysis for NOX1 expression as described above.

Statistical Analysis

Statistical analyses were performed using GraphPad Prism 10.6.0 (GraphPad Software, San Diego, CA). Normality was assessed using the Shapiro-Wilk test for data sets with n≥6; normally distributed data were analyzed using parametric tests, while nonnormally distributed data or data sets with n<6 were analyzed using nonparametric tests.

For 2-group comparisons, the Student *t* test was used for normally distributed data with equal variances (determined by the F-test), the Welch *t* test for normally distributed data with unequal variances, and the Mann-Whitney *U* test for nonparametric data. For comparisons involving ≥3 groups with n≥6, variance homogeneity was assessed using the Brown-Forsythe test, and 1-way ANOVA or 2-way ANOVA (for 2 independent factors) with the Tukey or Newman-Keuls multiple comparison test was used or nonparametric data with the Kruskal-Wallis test followed by the Dunn post hoc test. For comparisons involving 4 groups with n<6, aligned rank transform ANOVA followed by 2-tailed Welch *t* tests was used (eg, for data in Figure 1F, when a 2-group comparison between WT and NOX1 gKO mice under a high-fat diet is the data to be analyzed).

For experiments with repeated measurements with n≥6, overall effects were assessed by 2-way repeated-measures ANOVA, and differences at individual time points were evaluated using 2-way ANOVA with the Tukey or Newman-Keuls post hoc test. For experiments with repeated measurements with n<6, a mixed-effects model (restricted maximum likelihood [REML]) with the Dunnett or Holm-Šídák multiple comparison tests was used. Nonlinear regression (nonlinear curve fitting) was applied to analyze relaxation responses. Post hoc pairwise comparisons were adjusted for multiple testing, and statistical significance was defined as 2-sided $P<0.05$.

RESULTS

Global NOX1 Knockout Selectively Attenuates High-Fat Feeding–Induced Obesity and Metabolic Syndrome

We have previously demonstrated that vascular-driven ROS production mediates high-fat-diet–induced obesity and metabolic syndrome, establishing a paradigm-shifting concept that vascular ROS function serves as a causal factor, rather than a consequence, for/of the development of obesity and metabolic syndrome. Overexpression of $p22^{phox}$ in the vascular cells results in activation of NOX and consequent skeletal mitochondrial dysfunction to result in impaired spontaneous

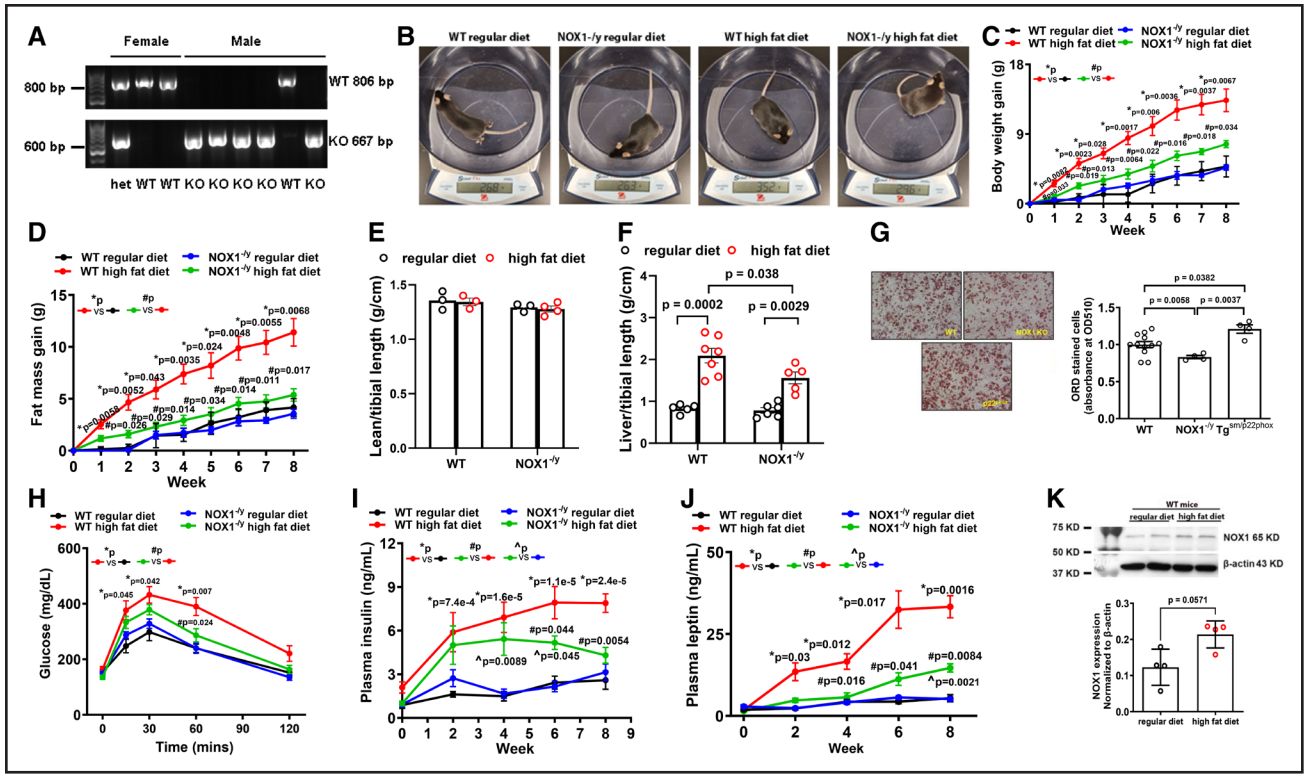

Figure 1. Global knockout of NOX1 (NADPH oxidase isoform 1) attenuated high-fat-diet–induced obesity and metabolic syndrome.

A, Genotyping of NOX1 (X-link) mice. Male WT: wild type (806 bp). Male KO: knockout (667 bp). Male NOX1 global knockout mice and WT littermate controls of 8 weeks of age were fed a high-fat diet (42% calories from fat) or a regular diet for 8 weeks. **B**, Representative images of mice of different groups with changes in body weight after 8 weeks of high-fat feeding. Body weight was markedly increased in high-fat–fed WT mice, which was substantially attenuated by global knockout of NOX1. Body weight and tissue mass were determined weekly using EchoMRI. **C**, Weekly changes in body weight of different groups, indicating that high-fat-diet–induced body weight gain was substantially alleviated in NOX1 global knockout mice starting from week 2. n=5 for the WT regular diet group; n=6 mice for the NOX1$^{-/y}$ regular diet group; n=5 for the WT high-fat-diet group; and n=6 for the NOX1$^{-/y}$ high-fat-diet group. **D**, Weekly changes in fat mass indicating that high-fat-diet–induced adipose tissue accumulation was near completely attenuated in NOX1 global knockout mice. n=5 for the WT regular diet group; n=6 for the NOX1$^{-/y}$ regular diet group; n=5 for the WT high-fat-diet group; and n=6 for the NOX1$^{-/y}$ high-fat-diet group. **E**, Lean mass normalized to tibial length, indicating no change after 8 weeks of high-fat feeding in all experimental groups. n=3 for the WT regular diet group; n=3 for the NOX1$^{-/y}$ regular diet group; n=3 for the WT high-fat-diet group; and n=4 for the NOX1$^{-/y}$ high-fat-diet group. **F**, Liver weight normalized to tibial length indicating development of fatty liver in high-fat–fed WT mice, which was markedly abrogated in NOX1 global knockout mice. n=5 for the WT regular diet group; n=6 for the NOX1$^{-/y}$ regular diet group; n=7 for the WT high-fat-diet group; and n=5 for the NOX1$^{-/y}$ high-fat-diet group. **G**, Preadipocyte differentiation data indicating reduced differentiation in preadipocytes isolated from NOX1 global knockout mice fed a high-fat diet but elevated differentiation in mice overexpressing vascular p22^{phox} (cytochrome b-245 alpha chain). Preadipocytes were isolated from the inguinal adipose tissue depot, differentiated into mature adipocytes, and stained with Oil Red O (ORO). After the staining, ORO was extracted for the determination of absorbance at 510 nm. n=12 for the WT group; n=4 for the NOX1$^{-/y}$ group; and n=4 for the Tg$^{sm/p22phox}$ group. **H**, Results of glucose tolerance tests indicating significantly increased glucose intolerance in high-fat–fed WT mice, which was substantially alleviated by NOX1 global knockout. n=3 for the WT regular diet group; n=4 for the NOX1$^{-/y}$ regular diet group; n=8 for the WT high-fat-diet group; and n=6 for the NOX1$^{-/y}$ high-fat-diet group. **I**, Plasma insulin levels indicating markedly increased circulating levels of insulin in high-fat–fed WT mice, which were substantially diminished by NOX1 global knockout. n=5 for the WT regular diet group; n=5 for the NOX1$^{-/y}$ regular diet group; n=8 for the WT high-fat-diet group; and n=5 for the NOX1$^{-/y}$ high-fat-diet group. **J**, Plasma leptin levels indicating markedly increased circulating levels of leptin in high-fat–fed WT mice, which were nearly completely attenuated by NOX1 global knockout mice. n=5 for the WT regular diet group; n=6 mice for the NOX1$^{-/y}$ regular diet group; n=5 for the WT high-fat-diet group; and n=5 for the NOX1$^{-/y}$ high-fat-diet group. **K**, Upregulation of NOX1 protein expression in high-fat–fed WT mice. The WT mice were fed a high-fat diet as described, and the aortas were freshly isolated for the determination of NOX1 protein expression by Western blotting. n=4 for each group. **C**, **D**, **I**, and **J** were assessed by a mixed-effects model (restricted maximum likelihood [REML]) with the Dunnett multiple comparisons tests. **E** and **F** were assessed by aligned rank transform (ART) ANOVA followed by planned comparisons using the 2-tailed Welch *t* tests. **G** was analyzed using 1-way ANOVA with the Dunnett T3 multiple comparisons test. **H** was assessed by mixed-effects model (REML) with the Holm-Šídák multiple comparisons test. **K** was analyzed using the Mann-Whitney *U* test. Data are shown as mean±SEM. All of the specific *P* values have been included in each graph figure.

activity and energy expenditure.[8] Of note, all of the NOX isoforms, except for NOX5 that is not present in rodents, require p22^{phox} for enzymatic activation.[11] NOX3 is expressed primarily in the inner ear.[11] Therefore, we next examined direct causal role(s) of NOX isoforms (NOX1, NOX2, and NOX4) in mediating high-fat

feeding–induced obesity and metabolic syndrome, employing high-fat–fed global knockout mice with deletion in NOX1, NOX2, or NOX4. As shown in Figure 1, in NOX1 global knockout mice, verified by genotyping (Figure 1A), high-fat-diet–induced body weight gain was substantially attenuated (Figure 1B and 1C). However, body weight gain was not affected by NOX2 global knockout (Figure S1A), while NOX4 global knockout increased body weight by contrast in response to high-fat feeding (Figure S2A). Consistent with decreased body weight gain, adipose mass gain was also reduced almost to regular diet levels in high-fat–fed NOX1 global knockout mice (Figure 1D), while lean mass was not different between high-fat–fed NOX1 global knockout and WT littermate groups (Figure 1E). High-fat-diet–induced increase in liver weight was also markedly attenuated in NOX1 global knockout mice (Figure 1F). Of note, organ weights of lung, spleen, and kidney were not affected by high-fat feeding or regulated in NOX1 global knockout mice, while NOX1 global knockout also had no effects on elevated heart weights in response to high-fat feeding (Figure S3A through S3E). In addition, primary preadipocytes were isolated from high-fat–fed WT, NOX1 global knockout, and $tg^{sm/p22phox}$ mice. Cultured preadipocytes were induced to differentiate using a differentiation cocktail, and adipocyte differentiation activity was analyzed as described in the Methods section. As shown in Figure 1G, NOX1 deletion significantly attenuated preadipocyte differentiation, which is consistent with reduced fat mass gain in vivo. On the contrary, preadipocytes from high-fat–fed $tg^{sm/p22phox}$ mice had increased adipogenesis (Figure 1G).

We next examined whether global NOX1 deletion is able to modify metabolic parameters under high-fat feeding. We examined glucose clearance rate in high-fat–fed animals. As shown in Figure 1H, intraperitoneal glucose challenge revealed a marked delay in glucose clearance or increase in glucose intolerance in high-fat–fed WT mice compared with the regular diet group, while NOX1 global knockout substantially attenuated this response. However, high-fat–fed NOX2 global knockout mice (Figure S1B) and NOX4 global knockout mice (Figure S2B) displayed no difference from high-fat–fed WT mice in glucose intolerance. Of note, circulating insulin and leptin levels were significantly upregulated in high-fat–fed WT mice compared with the regular diet group (Figure 1I and 1J). NOX1 global deletion in mice, however, markedly attenuated plasma insulin levels at 6 and 8 weeks (Figure 1I) and leptin levels at 2, 4, 6, and 8 weeks (Figure 1J). Importantly, NOX1 protein expression was indeed markedly upregulated in high-fat–fed WT mice (Figure 1K).

Taken together, these results clearly demonstrate that NOX1, instead of NOX2 or NOX4, selectively mediates high-fat feeding–induced obesity and metabolic syndrome in mice.

Endothelial-Specific Deletion of NOX1 Abrogates High-Fat Feeding–Induced Obesity and Metabolic Syndrome

We have shown that NOX-derived vascular ROS play a causal role in the development of obesity and metabolic syndrome,[8] and that NOX1 deletion robustly alleviates high-fat feeding–induced phenotypes of obesity and metabolic syndrome as described above. NOX1 is expressed in ECs, smooth muscle cells, and cardiomyocytes in the cardiovascular system.[11] Based on our previous findings that NOX activation impairs skeletal muscle mitochondrial function, hence impairing spontaneous activity,[8] we hypothesize that vascular NOX1 activation drives initial ROS production under high-fat feeding and consequent ROS-dependent triggering of mitochondrial dysfunction in nearby skeletal muscle. To dissect the specific cell/tissue type in the vasculature that is specifically involved in NOX1-driven development of obesity and metabolic syndrome, we generated endothelial or VSMC-specific NOX1 knockout mice for the first time in-house and subjected the animals to high-fat feeding.

To induce cell type–specific knockout of NOX1, we first created a Cre-inducible NOX1 knockout gene construct by inserting an orphan loxP site and an FRT-neo-FRT-loxP resistance cassette inserted into the NOX1 genomic locus to target exon 3 to exon 8 (E3–E8) of NOX1 (Figure 2A). The floxed NOX1 founders were verified by genotyping (Figure 2B) and backcrossed in-house to the C57BL/6 background for >10 generations. Then, the mice were crossed with Cdh5Cre mice,[31] which were also verified by genotyping (Figure 2B) to generate endothelial-specific NOX1 knockout mice (Cdh5Cre-NOX1CKO mice). Using EC washout experiments as we previously published to examine EC-specific gene expression, we found that NOX1 expression was successfully knocked out in Cdh5Cre-NOX1CKO mice compared with the littermate controls (Figure 2C). NOX1 expression was only blunted in the EC fraction but not in the EC-denuded aortic fraction (Figure 2C). eNOS (endothelial nitric oxide synthase) was used as an internal control for successful isolation of ECs from the aortas, with it being present only in the EC fraction (Figure 2C).

Eight-week-old Cdh5Cre-NOX1CKO mice and littermate controls were subjected to a high-fat diet or a regular diet for 8 weeks. As shown in Figure 2D and 2E, compared with Cdh5Cre-WT littermates, high-fat feeding–induced body weight gain was completely attenuated in Cdh5Cre-NOX1CKO mice, to the baseline as in regular diet–fed mice. Consistent with decreased body weight gain, adipose mass gain was also substantially lower in high-fat–fed Cdh5Cre-NOX1CKO mice (Figure 2F and 2G), while lean mass was not different between the Cdh5Cre-NOX1CKO and Cdh5Cre-WT

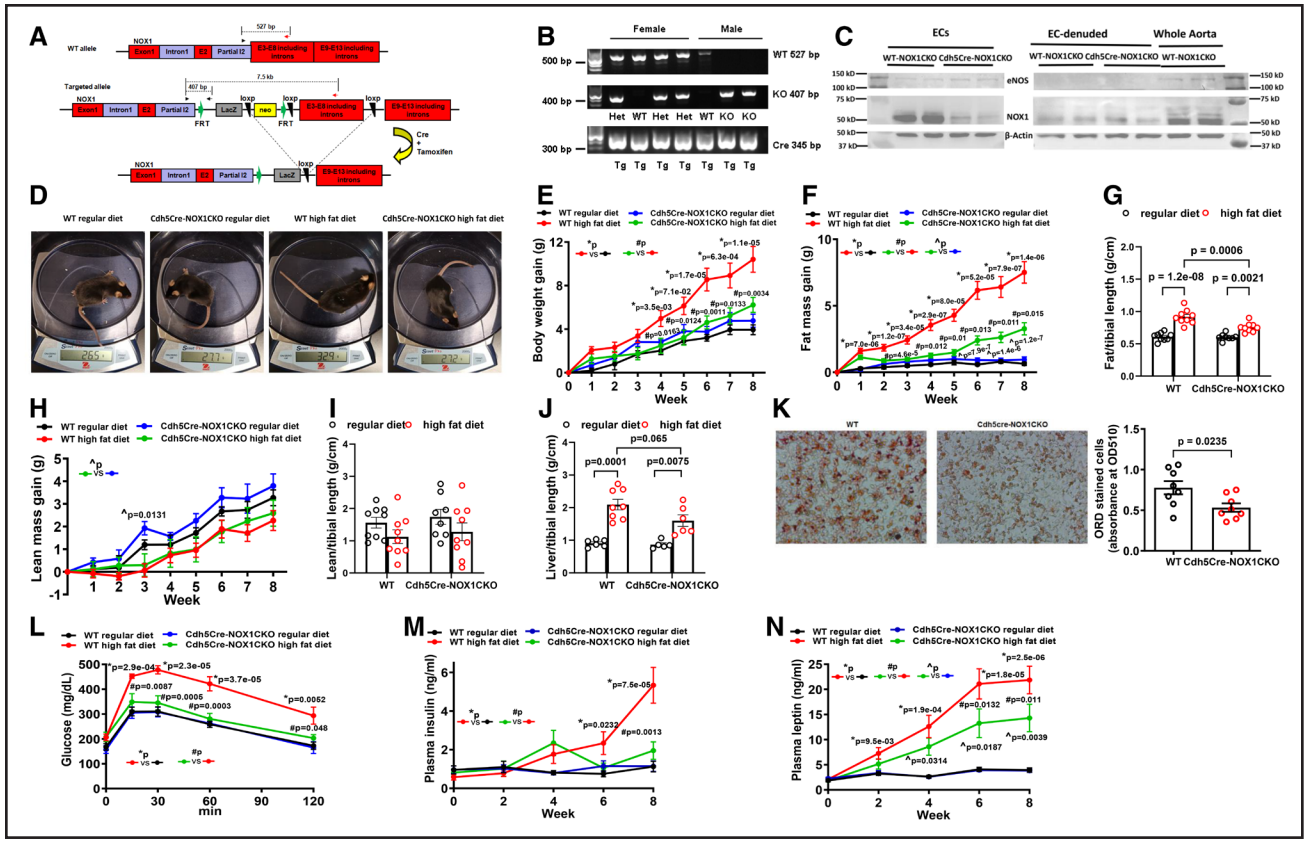

Figure 2. Endothelial-specific NOX1 (NADPH oxidase isoform 1) knockout attenuated high-fat-diet–induced obesity and metabolic syndrome.

A, Gene targeting strategy for the generation of NOX1-floxed mice (cre-inducible NOX1$^{flox/flox}$ knockout/floxed mice) showing the position of the loxP (locus of X-over P1 sites recognized by Cre recombinase) sequences (black inverted triangle) within the gene targeting construct before and after exons 3 to 8 (E3–E8) of NOX1. The floxed mice were crossed with endothelial cell (EC) cre mice of Cdh5 (cadherin 5; PAC [P1 artificial chromosome])-CreERT2 (Cre recombinase–estrogen receptor T2 fusion protein [tamoxifen-inducible Cre recombinase]) to generate Cdh5cre (cadherin 5 [vascular endothelial cadherin] promoter–driven Cre recombinase [endothelial-specific Cre expression])-NOX1CKO mice for endothelial-specific deletion of NOX1. **B**, Genotyping of Cdh5cre-NOX1CKO mice. WT: wild type (527 bp). KO: knockout (407 bp). Cdh5cre: 345 bp (homozygotes). Male Cdh5Cre mice (Cdh5cre-NOX1CKO and WT) were injected with tamoxifen at 5 weeks old and then fed with a high-fat diet (42% calories from fat) or a regular diet at the age of 8 weeks for 8 weeks. **C**, EC washout experiments indicating selective knockout of NOX1 in ECs isolated from mouse aortas, while the expression of NOX1 did not change in EC-denuded aortas. eNOS (endothelial nitric oxide synthase) expression was used to serve as a control for successful isolation of ECs without contamination from the EC-denuded fraction. **D**, Representative images of mice from Cdh5Cre-WT and Cdh5Cre-NOX1CKO groups fed with a regular diet or a high-fat diet for 8 weeks. Body weight was markedly increased in high-fat–fed Cdh5Cre-WT mice, which was substantially attenuated in Cdh5Cre-NOX1CKO mice with endothelial-specific deletion of NOX1. Body weight and tissue mass were determined weekly using EchoMRI. **E**, Weekly changes in body weight of different groups, indicating that high-fat-diet–induced body weight gain was substantially alleviated in endothelial-specific NOX1 knockout mice starting from week 4. n=9 for the WT regular diet group; n=8 for the Cdh5Cre-NOX1CKO regular diet group; n=9 for the WT high-fat-diet group; and n=9 for the Cdh5Cre-NOX1CKO high-fat-diet group. **F**, Weekly changes in fat mass indicating that high-fat-diet–induced adipose tissue accumulation was nearly completely attenuated in Cdh5Cre-NOX1CKO mice. n=9 for the WT regular diet group; n=8 for the Cdh5Cre-NOX1CKO regular diet group; n=9 for the WT high-fat-diet group; and n=9 for the Cdh5Cre-NOX1CKO high-fat-diet group. **G**, Fat mass normalized to tibial length, indicating that high-fat-diet–induced increase in fat mass in Cdh5Cre-WT mice was markedly abrogated in Cdh5Cre-NOX1CKO mice. n=9 for the WT regular diet group; n=8 for the Cdh5Cre-NOX1CKO regular diet group; n=9 for the WT high-fat-diet group; and n=9 for the Cdh5Cre-NOX1CKO high-fat-diet group. **H**, Weekly changes in lean mass indicating that lean mass gain was not changed in high-fed mice of different groups, except for one data point. n=9 for the WT regular diet group; n=8 for the Cdh5Cre-NOX1CKO regular diet group; n=9 for the WT high-fat-diet group; and n=9 for the Cdh5Cre-NOX1CKO high-fat-diet group. **I**, Lean mass normalized to tibial length, indicating no change after 8 weeks of high-fat feeding in all experimental groups. n=9 for the WT regular diet group; n=8 for the Cdh5Cre-NOX1CKO regular diet group; n=9 for the WT high-fat-diet group; and n=9 for the Cdh5Cre-NOX1CKO high-fat-diet group. **J**, Liver weight normalized to tibial length indicating development of fatty liver in high-fat–fed Cdh5Cre-WT mice, which was markedly alleviated in Cdh5Cre-NOX1CKO mice. n=6 for the WT regular diet group; n=5 for the Cdh5Cre-NOX1CKO regular diet group; n=8 for the WT high-fat-diet group; and n=6 for the Cdh5Cre-NOX1CKO high-fat-diet group. **K**, Preadipocyte differentiation data indicating markedly attenuated differentiation in preadipocytes isolated from Cdh5Cre-NOX1CKO mice fed a high-fat diet. Preadipocytes were isolated from the inguinal adipose tissue depot, differentiated into mature adipocytes, and stained with Oil Red O (ORO). After the staining, ORO was extracted for the determination of absorbance at 510 nm. n=8 per group. **L**, Results of glucose tolerance tests indicating significantly increased glucose intolerance in high-fat–fed Cdh5Cre-WT mice, which was abolished in Cdh5Cre-NOX1CKO mice. n=8 for the WT regular diet group; n=6 for the Cdh5Cre-NOX1CKO regular diet group; n=9 for the WT high-fat-diet group; and n=8 for the Cdh5Cre-NOX1CKO high-fat-diet group. **M**, Plasma insulin levels indicating markedly increased (*Continued*)

littermate groups after high-fat feeding (Figure 2H and 2I). In addition to decreased fat mass gain, we also observed markedly attenuated liver weight in high-fat–fed Cdh5Cre-NOX1CKO mice compared with their Cdh5Cre-WT littermates (Figure 2J), whereas organ weights of heart, lung, spleen, and kidney were not affected by endothelial-specific NOX1 knockout (Figure S4A through S4E). Endothelial-specific NOX1 deletion also significantly attenuated preadipocyte differentiation (Figure 2K), which is consistent with reduced fat mass gain in vivo.

We further examined metabolic parameters in high-fat–fed endothelial-specific NOX1 knockout mice. As shown in Figure 2L, intraperitoneal glucose challenge revealed that endothelial-specific NOX1 deletion completely attenuated high-fat feeding–induced glucose intolerance to the levels in regular diet–fed animals. In addition, endothelial-specific NOX1 deletion in mice abrogated elevations in plasma insulin levels at 8 weeks (Figure 2M) and that in plasma leptin levels at 6 and 8 weeks (Figure 2N).

Taken together, these results for the first time demonstrate that NOX1 situated in the ECs plays an important role in mediating high-fat-diet–induced obesity and metabolic syndrome in mice.

Smooth Muscle–Specific Deletion of NOX1 Has No Effect on High-Fat Feeding–Induced Obesity and Metabolic Syndrome

NOX1 is expressed in ECs and vascular smooth muscle cells in the vasculature.[11] NOX1 in either cell type can be activated first to potentially transduce ROS signals to provoke mitochondrial dysfunction in adjacent skeletal muscle. Therefore, we also examined whether specific deletion of NOX1 in smooth muscle cells has any effects on high-fat feeding–induced obesity and metabolic syndrome. NOX1 floxed mice were crossed with Myh-11Cre mice to generate smooth muscle–specific NOX1 knockout mice (Myh11Cre-NOX1CKO mice) for the first time, which were verified by genotyping (Figure S5A). As shown in Figure S5B through S5E, body weight gain and fat mass gain in Myh11Cre-NOX1CKO and Myh11Cre-NOX1WT mice were significantly and equally increased in response to high-fat feeding compared with chew diet–fed Myh11Cre-NOX1CKO and Myh11Cre-NOX1WT mice, respectively. Notably, lean mass was increased in Myh11Cre-NOX1CKO mice compared with Myh11Cre-WT littermates after high-fat feeding for 4 to 8 weeks (Figure S5F and S5G), but there was no significant change when normalized to the tibial length.

We also examined whether smooth muscle–specific NOX1 deletion was able to modify metabolic parameters under high-fat feeding. As shown in Figure S5H, intraperitoneal glucose challenge revealed equally impaired glucose tolerance in high-fat–fed Myh11Cre-NOX1CKO and Myh11Cre-NOX1WT mice compared with regular diet–fed Myh11Cre-NOX1CKO and Myh11Cre-NOX1WT mice, respectively. In addition, high-fat feeding resulted in similar phenotypes of insulin and leptin resistance in both Myh11Cre-NOX1CKO mice and Myh11Cre-WT mice (Figure S5I and S5J). Of note, no evidence is available on NOX1 regulation in vascular smooth muscle cells of human obese subjects, indicating potential irrelevance of its regulation. Taken together, these data indicate that smooth muscle–specific NOX1 ablation in mice has no effect on phenotypes of obesity and metabolic syndrome. Therefore, NOX1 activation in ECs, rather than in smooth muscle cells, plays a specific and selective causal role in mediating high-fat-diet–induced obesity and metabolic syndrome in mice.

Endothelial-Specific NOX1 Transgenesis Induces Exaggerated Obesity and Metabolic Syndrome in Response to High-Fat Feeding

To further evaluate the intermediate role of endothelial NOX1 in high-fat feeding–induced obesity and metabolic syndrome, cre-inducible NOX1 knockin/floxed mice were generated for the first time in-house, as described in Figure 3A, and backcrossed to the C57BL/6 background for >10 generations. Then, the mice were crossed with Cdh5Cre mice to generate endothelial-specific NOX1 knockin (Cdh5Cre-NOX1CKI mice) mice, which were verified by genotyping (Figure 3B). Using EC washout experiments as we previously published to examine EC-specific gene expression, we found that NOX1 expression was successfully knocked in in Cdh5Cre-NOX1CKO mice compared with the littermate controls (Figure 3C). NOX1 expression was only enhanced in the EC fraction but not in the EC-denuded aortic fraction (Figure 3C). eNOS was used as an internal control for successful

Figure 2 Continued. circulating levels of insulin in high-fat–fed Cdh5Cre-WT mice, which were nearly completely diminished in Cdh5Cre-NOX1CKO mice. n=9 for the WT regular diet group; n=8 for the Cdh5Cre-NOX1CKO regular diet group; n=10 for the WT high-fat-diet group; and n=9 for the Cdh5Cre-NOX1CKO high-fat-diet group. **N**, Plasma leptin levels indicating markedly increased circulating levels of leptin in high-fat–fed Cdh5Cre-WT mice, which were markedly attenuated in Cdh5Cre-NOX1CKO mice. n=8 for the WT regular diet group; n=9 for the Cdh5Cre-NOX1CKO regular diet group; n=9 for the WT high-fat-diet group; and n=8 for the Cdh5Cre-NOX1CKO high-fat-diet group. For **E**, **F**, **H**, and **L** through **N**, overall effects were assessed by 2-way repeated-measures ANOVA, and differences at individual time points were evaluated using 2-way ANOVA with the Tukey or Newman-Keuls post hoc testing. **G** was analyzed using 2-way ANOVA with the Tukey post hoc test. **I** was analyzed using 2-way ANOVA with the Newman-Keuls post hoc test. **J** was assessed by aligned rank transform (ART) ANOVA followed by planned comparisons using the 2-tailed Welch *t* tests. **K** was analyzed using an unpaired *t* test. Data are shown as mean±SEM. All of the specific *P* values have been included in each graph figure.

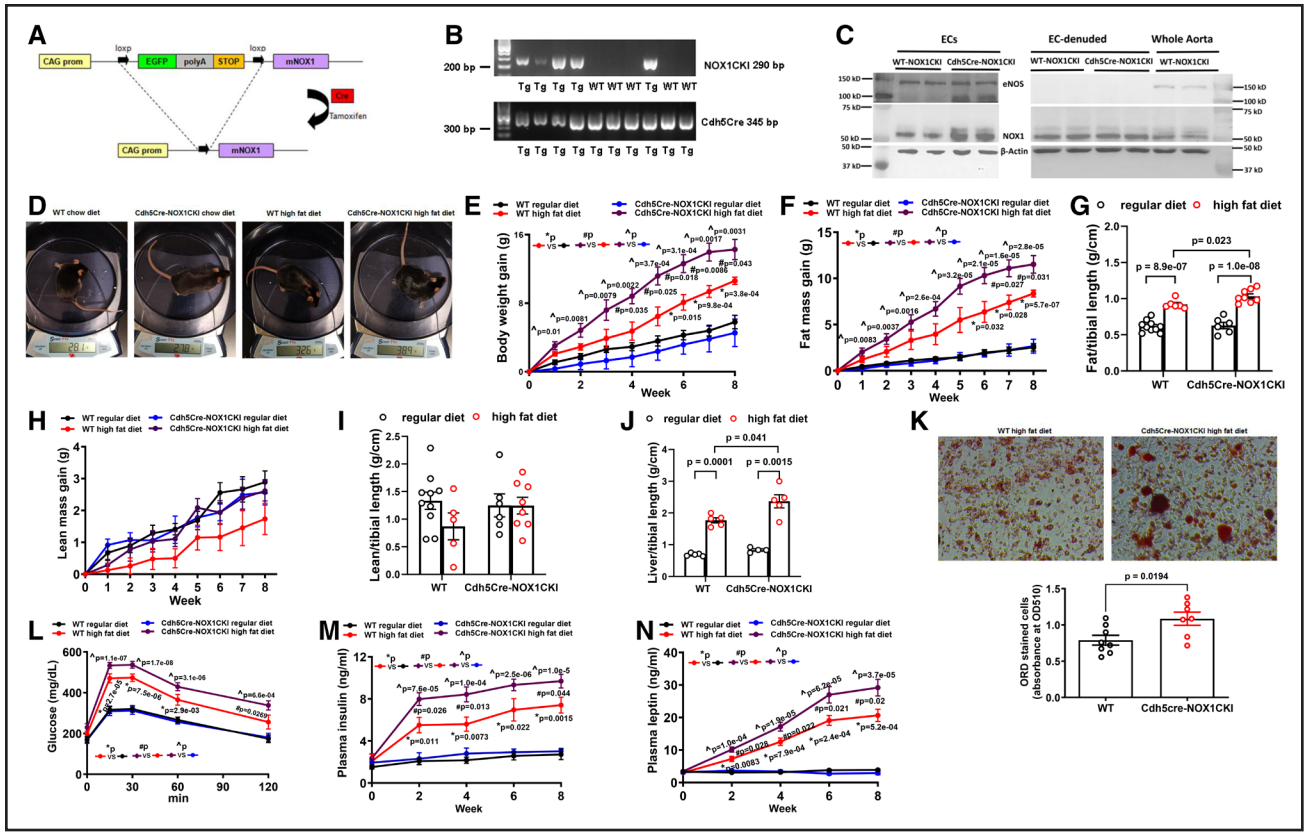

Figure 3. Endothelial-specific transgenesis of NOX1 (NADPH oxidase isoform 1) exacerbated high-fat-diet–induced obesity and metabolic syndrome.

A, Gene targeting strategy for the generation of cre-inducible NOX1$^{flox/flox}$ knockin/floxed mice. **B**, Genotyping of Cdh5cre (cadherin 5 [vascular endothelial cadherin] promoter–driven Cre recombinase [endothelial-specific Cre expression])-NOX1CKI mice. The cre-inducible NOX1$^{flox/flox}$ knockin/floxed mice were crossed with Cdh5cre mice to generate Cdh5cre-NOX1CKI mice for endothelial-specific transgenesis of NOX1. NOX1CKI: 290 bp. Cdh5cre: 345 bp. Male Cdh5cre mice (Cdh5cre-NOX1CKI and wild type [WT]) were injected with tamoxifen at 5 weeks old and then fed a high-fat diet (42% calories from fat) or a regular diet at the age of 8 weeks for 8 weeks. **C**, Endothelial cell (EC) washout experiments indicating selective knockin of NOX1 in ECs isolated from mouse aortas, while the expression of NOX1 did not change in EC-denuded aortas. eNOS (endothelial nitric oxide synthase) expression was used to serve as a control for successful isolation of ECs without contamination from the EC-denuded fraction. **D**, Representative images of mice from Cdh5Cre-WT and Cdh5cre-NOX1CKI groups fed with a regular diet or high-fat diet after 8 weeks. Body weight was substantially further increased in high-fat–fed Cdh5cre-NOX1CKI mice with endothelial-specific NOX1 transgenesis compared with the Cdh5Cre-WT controls. **E**, Weekly changes in body weight of different groups, indicating that high-fat-diet–induced exaggerated body weight gain in endothelial-specific NOX1 transgenic mice starting from week 3. n=10 for the WT regular diet group; n=5 for Cdh5Cre-NOX1CKI regular diet group; n=6 for the WT high-fat-diet group; and n=8 for Cdh5Cre-NOX1CKI high-fat-diet group. EchoMRI was used to detect body weight and tissue mass weekly. **F**, Weekly changes in fat mass indicating that high-fat-diet–induced exaggerated adipose tissue accumulation in Cdh5cre-NOX1CKI mice. n=10 for the WT regular diet group; n=5 for Cdh5Cre-NOX1CKI regular diet group; n=6 for the WT high-fat-diet group; and n=8 for Cdh5Cre-NOX1CKI high-fat-diet group. **G**, Fat mass normalized to tibial length, indicating that high-fat-diet–induced increase in fat mass in Cdh5Cre-WT mice was further elevated in Cdh5cre-NOX1CKI mice. n=10 or WT regular diet group; n=6 or Cdh5Cre-NOX1CKI regular diet group; n=6 for the WT high-fat-diet group; and n=8 for Cdh5Cre-NOX1CKI high-fat-diet group. **H**, Weekly changes in lean mass indicating that lean mass gain was not different between high-fat–fed Cdh5cre-NOX1CKI mice and high-fat–fed Cdh5Cre-WT mice. n=10 for the WT regular diet group; n=5 for Cdh5Cre-NOX1CKI regular diet group; n=6 for the WT high-fat-diet group; and n=8 for Cdh5Cre-NOX1CKI high-fat-diet group. **I**, Lean mass normalized to tibial length, indicating the same lean mass between high-fat–fed Cdh5cre-NOX1CKI mice and high-fat–fed Cdh5Cre-WT mice at week 8. n=10 for the WT regular diet group; n=5 for Cdh5Cre-NOX1CKI regular diet group; n=6 for the WT high-fat-diet group; and n=8 for Cdh5Cre-NOX1CKI high-fat-diet group. **J**, Liver weight normalized to tibial length indicating development of fatty liver in high-fat–fed Cdh5Cre-WT mice, which was further exaggerated in high-fat–fed Cdh5cre-NOX1CKI mice. n=6 for the WT regular diet group; n=5 for Cdh5Cre-NOX1CKI regular diet group; n=6 for the WT high-fat-diet group; and n=6 for Cdh5Cre-NOX1CKI high-fat-diet group. **K**, Preadipocyte differentiation data indicating markedly further elevated differentiation in preadipocytes isolated from Cdh5cre-NOX1CKI mice fed a high-fat diet. Preadipocytes were isolated from the inguinal adipose tissue depot, differentiated into mature adipocytes, and stained with Oil Red O (ORO). After the staining, ORO was extracted for the determination of absorbance at 510 nm. n=8 for WT; n=7 or Cdh5Cre-NOX1CKI regular diet group. **L**, Results of glucose tolerance tests indicating significantly further deteriorated glucose intolerance in high-fat–fed Cdh5cre-NOX1CKI mice compared with high-fat–fed Cdh5Cre-WT mice. n=10 for the WT regular diet group; n=6 for Cdh5Cre-NOX1CKI regular diet group; n=6 for the WT high-fat-diet group; and n=8 for Cdh5Cre-NOX1CKI high-fat-diet group. **M**, Plasma insulin levels indicating significantly further deteriorated insulin resistance in high-fat–fed Cdh5cre-NOX1CKI mice compared with high-fat–fed Cdh5Cre-WT mice. n=10 for the WT regular diet group; n=5 for Cdh5Cre-NOX1CKI regular diet group; n=6 for the WT high-fat-diet group; and n=8 for Cdh5Cre-NOX1CKI high-fat-diet group. **N**, Plasma leptin levels indicating significantly further (*Continued*)

isolation of ECs from the aortas, with it being present only in the EC fraction (Figure 3C).

Eight-week-old Cdh5Cre-NOX1CKI and littermate control mice were subjected to a high-fat diet or a regular diet for 8 weeks. As shown in Figure 4D and 4E, body weight gain of Cdh5Cre-NOX1CKI mice was significantly further increased compared with that of Cdh5Cre-WT littermates on a high-fat diet. Consistently, adipose mass gain was also significantly further increased in high-fat–fed Cdh5Cre-NOX1CKI mice (Figure 3F and 3G), while lean mass was not different between Cdh5Cre-NOX1CKI and Cdh5Cre-WT littermate groups (Figure 3H and 3I). Of note, liver weight in high-fat–fed Cdh5Cre-NOX1CKI mice was also significantly higher than that of high-fat–fed Cdh5Cre-WT littermates (Figure 3J), whereas organ weights of heart, lung, spleen, and kidney were not different in endothelial-specific NOX1 knockin mice compared with control littermates (Figure S6A through S6E). Furthermore, preadipocytes isolated from high-fat–fed Cdh5Cre-NOX1CKI mice had a significantly higher differentiation rate compared with that of Cdh5Cre-WT littermate mice fed a high-fat diet (Figure 3K), which is consistent with further increased fat mass gain in vivo.

In addition, high-fat–fed Cdh5Cre-NOX1CKI mice displayed more severely delayed glucose clearance compared with Cdh5Cre-WT littermates (Figure 3L). High-fat–fed Cdh5Cre-NOX1CKI mice also had further increased plasma insulin levels at 2, 4, 6, and 8 weeks (Figure 3M) and further elevated leptin levels at 4, 6, and 8 weeks (Figure 3N).

Taken together, these results additionally confirm that endothelial-specific activation of NOX1 plays a vital role in mediating high-fat feeding–induced obesity and metabolic syndrome.

NOX1 Global Knockout Abrogates Obesity and Metabolic Syndrome via Preservation of Skeletal Function to Maintain Spontaneous Activity and Exercise Capacity

Because NOX1 global knockout and WT mice had similar energy and water intake during high-fat feeding (Figure 4A and 4B), we examined whether energy expenditure was altered in high-fat–fed NOX1 global knockout mice by measuring spontaneous activity and exercise capacity. We assessed the spontaneous activity of regular diet–fed or high-fat-diet–fed animals using an infrared video monitoring system as we previously published.[8] Of note, spontaneous activity was increased in NOX1 global knockout mice at baseline when fed a regular diet (Figure 4C). High-fat feeding markedly reduced spontaneous activity in WT littermates, which was completely restored to more than baseline in NOX1 global knockout mice (Figure 4C), indicating robust protective effects of NOX1 deletion in preserving spontaneous activity to maintain normal energy expenditure during high-fat feeding. To further evaluate exercise capacity in high-fat–fed NOX1 global knockouts versus WT littermates, we used a mouse treadmill to measure exercise capacity, with parameters recorded for exhaustion time, exhaustion travel distance, and exhaustion speed for each animal. Compared with high-fat–fed WT littermates, NOX1 global knockout mice fed a high-fat diet displayed significantly longer exhaustion time, longer traveled distance, and higher exhaustion speed (Figure 4D through 4F, respectively). Importantly, the completely preserved spontaneous activity and much improved exercise capacity ensure sufficient energy expenditure to alleviate the development of obesity.

It is known that oxygen consumption is positively correlated with physical activity. We next examined real-time oxygen consumption in mice using metabolic cages (Oxymax-CLAMS; Columbus Instruments). We found that oxygen consumption was enhanced in high-fat–fed NOX1 global knockout mice compared with WT littermates (Figure 4G and 4H). The VCO_2 showed the same trend as for VO_2 (Figure 4I and 4J). These data indicate that NOX1 global knockout restores energy expenditure in high-fat–fed animals. The increased energy expenditure is attributed to completely preserved spontaneous activity and augmented exercise capacity as described above.

In addition, we examined ATP production by assessing skeletal muscle mitochondrial respiratory control ratio (RCR) using Seahorse. Skeletal muscle mitochondrial RCR was significantly decreased in high-fat–fed WT littermates, which was, however, completely recovered to baseline by NOX1 global knockout (Figure 4K). Given that RCR is an index of the tightness of coupling between respiration and phosphorylation, a higher value of RCR in NOX1 global knockout mice indicates a tighter link between the amount of O_2 consumed and the formation

Figure 3 Continued. deteriorated leptin resistance in high-fat–fed Cdh5cre-NOX1CKI mice compared with high-fat–fed Cdh5Cre-WT mice. n=10 for the WT regular diet group; n=5 for Cdh5Cre-NOX1CKI regular diet group; n=6 for the WT high-fat-diet group; and n=8 for Cdh5Cre-NOX1CKI high-fat-diet group. **E**, **F**, and **H** were assessed by a mixed-effects model (restricted maximum likelihood [REML]) with the Dunnett multiple comparisons tests. **M** and **N** were assessed by mixed-effects model (REML) with the Holm-Šídák multiple comparisons test. For **L**, overall effects were assessed by 2-way repeated-measures ANOVA, and differences at individual time points were evaluated using 2-way ANOVA with the Tukey post hoc testing. **G** was analyzed using 2-way ANOVA with the Newman-Keuls post hoc test. **I** and **J** were assessed by aligned rank transform (ART) ANOVA followed by planned comparisons using the 2-tailed Welch *t* tests. **K** was analyzed using an unpaired *t* test. Data are shown as mean±SEM. All of the specific *P* values have been included in each graph figure.

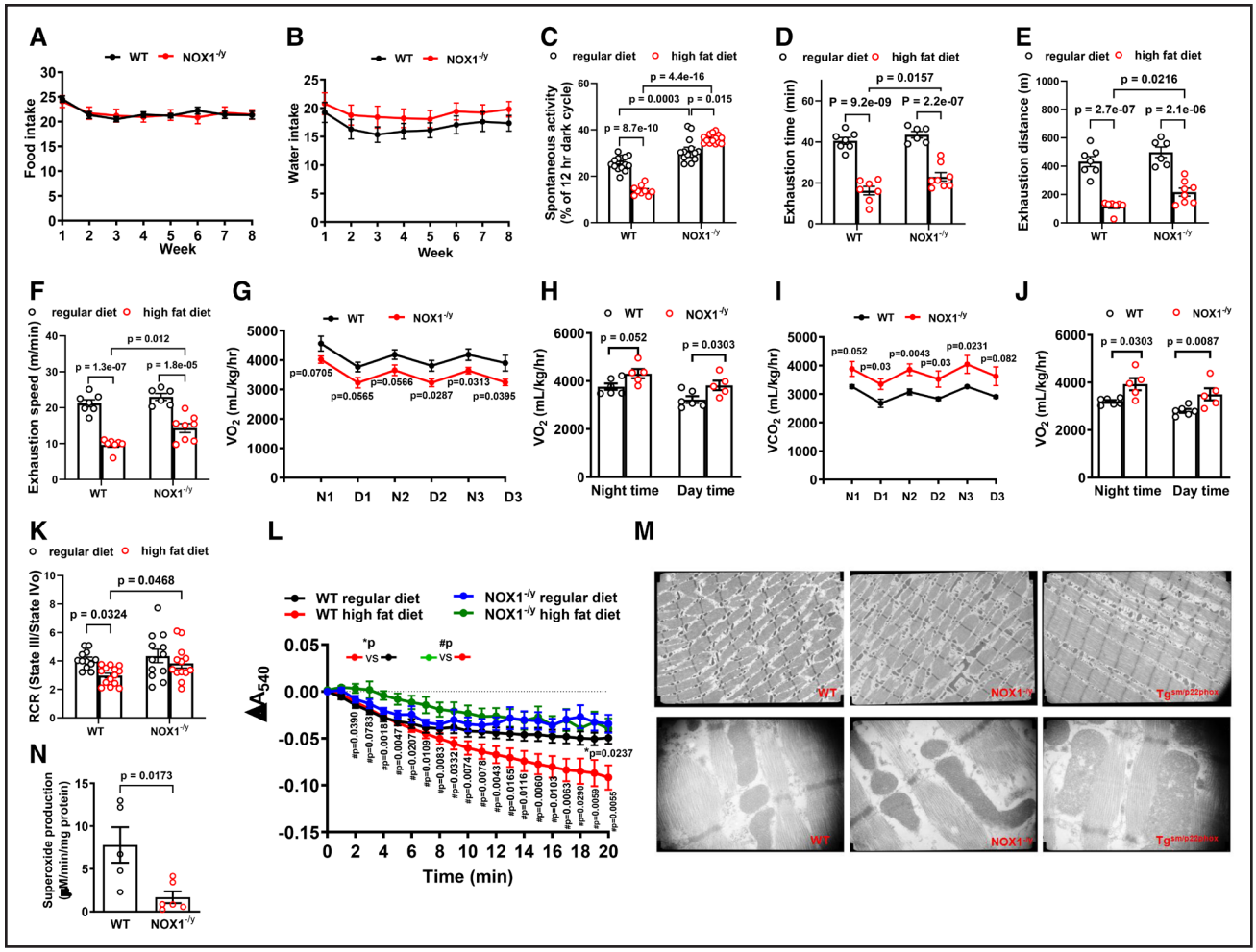

Figure 4. NOX1 (NADPH oxidase isoform 1) global knockout enhanced spontaneous activity and exercise capacity via preservation of skeletal mitochondrial function under high-fat feeding.

A, Grouped data of food intake in wild-type (WT) and NOX1 global knockout mice (NOX1$^{-/y}$) mice, indicating similar food intake between the 2 groups in response to a high-fat diet. n=8 per group. **B**, Grouped data of water intake in WT and NOX1$^{-/y}$ mice indicating similar water intake between the 2 groups in response to a high-fat diet. n=8 per group. **C**, Mouse spontaneous activity data indicating significantly reduced nighttime activity in high-fat–fed WT mice, which was markedly restored in NOX1$^{-/y}$ mice. n=9 for the WT regular diet group; n=14 for the NOX1$^{-/y}$ regular diet group; n=14 for the WT high-fat-diet group; and n=14 for the NOX1$^{-/y}$ high-fat-diet group. Mouse spontaneous activity was analyzed by a video monitoring system. In additional experiments, regular diet–fed and high-fat-diet–fed mice were assayed for exercise capacity using a mouse treadmill system. Exercise capacity was assessed by determining (**D**) exhaustion time, (**E**) total distance traveled at exhaustion, and (**F**) speed at exhaustion. By all 3 parameters, the exercise capacity was found markedly preserved in high-fat–fed NOX1$^{-/y}$ mice compared with WT controls. n=7 for the WT regular diet group; n=6 for the NOX1$^{-/y}$ regular diet group; n=7 for the WT high-fat-diet group; and n=8 for the NOX1$^{-/y}$ high-fat-diet group. **G**, Oxygen consumption data indicating preserved oxygen consumption in high-fat–fed NOX1$^{-/y}$, which varied normally with circadian rhythm. n=5 for WT; n=6 for NOX1$^{-/y}$. Oxygen consumption was measured using an Oxymax Comprehensive Lab Animal Monitoring System. **H**, Oxygen consumption during both nighttime and daytime was significantly improved in high-fat–fed NOX1$^{-/y}$ mice compared with WT controls. *P<0.05 compared with high-fat–fed WT. n=5 for WT; n=6 for NOX1$^{-/y}$. **I**, CO_2 production data indicating preserved levels of CO_2 production in high-fat–fed NOX1 global knockout mice, which varied normally with circadian rhythm. n=5 for WT; n=6 for NOX1$^{-/y}$. CO_2 production was measured using an Oxymax Comprehensive Lab Animal Monitoring System. **J**, CO_2 production during both nighttime and daytime was significantly improved in NOX1$^{-/y}$ mice fed a high-fat diet. n=5 for WT; n=6 for NOX1$^{-/y}$. **K**, Respiratory control ratio (RCR), determined in mitochondria freshly isolated from skeletal muscle using a Seahorse XF24-3 analyzer, was found markedly decreased in high-fat–fed WT mice, which was substantially restored in NOX1$^{-/y}$ mice. n=12 for the WT regular diet group; n=12 for the NOX1$^{-/y}$ regular diet group; n=14 for the WT high-fat-diet group; and n=13 for the NOX1$^{-/y}$ high-fat-diet group. Respirational capacity was measured in the XF24 cell culture microplates using a Seahorse XF 24-3 analyzer. **L**, Skeletal mitochondrial swelling data indicating completely reversed swelling activity in high-fat–fed NOX1$^{-/y}$ mice compared with WT controls. n=9 for the WT regular diet group; n=6 for the NOX1$^{-/y}$ regular diet group; n=7 for the WT high-fat-diet group; and n=8 for the NOX1$^{-/y}$ high-fat-diet group. Fresh mitochondria were isolated from skeletal muscle, and mitochondrial swelling was measured by monitoring the decrease in absorbance at 540 nm upon calcium stimulation. **M**, Representative images of mitochondria in soleus muscle examined by electron microscopy (EM) at resolution of ×2900 and ×7200, indicating disorganization of mitochondrial cristae in high-fat–fed WT, and further aggregated response in tg$^{sm/p22phox}$ mice, while this was completely reversed in high-fat–fed NOX1$^{-/y}$ mice. EM was used to examine mitochondrial cristae structures. **N**, Superoxide production data indicating substantially diminished mitochondrial superoxide production in skeletal muscle mitochondrial preparation from high-fat–fed NOX1$^{-/y}$ mice compared with high-fat–fed WT mice. n=5 for WT; n=6 for NOX1$^{-/y}$. An electron spin resonance (ESR) spectrometer was used to detect superoxide production from freshly prepared skeletal muscle (*Continued*)

of ATP, confirming that the mitochondria are functioning more efficiently in NOX1 global knockout mice. Likewise, calcium-induced mitochondrial swelling, as a readout of mitochondrial dysfunction, was significantly increased in high-fat–fed WT littermates, which was, however, completely attenuated in NOX1 global knockout mice (Figure 4L), indicating preserved mitochondrial integrity. In addition, we examined the cristae structure of the mitochondria in the soleus muscle by transmission electron microscopy. Notably, swollen mitochondria with perturbation of cristae structure were observed in $tg^{sm/p22phox}$ mice fed with a high-fat diet (Figure 4M). It has been reported that the oxidative phosphorylation system is organized in folded cristae.[36] Upon perturbation of cristae, the electron transport chain is less efficient, and mitochondrial performance will decrease. Importantly, the density and structure of mitochondrial cristae were fully restored in high-fat–fed NOX1 global knockout mice compared with that of WT littermates (Figure 4M), further indicating preserved mitochondrial respiratory performance. We also measured mitochondrial ROS production as one of the indicators of changes in mitochondrial function. As shown in Figure 4, skeletal muscle mitochondrial production of superoxide was significantly decreased in high-fat–fed NOX1 global knockout mice compared with WT littermates. Taken together, these data indicate that NOX1 ablation preserved spontaneous activity and exercise capacity via maintenance of skeletal muscle function attributed to preserved mitochondrial function, which was reflected by increased oxygen consumption and ATP production, reduced mitochondrial swelling activity and superoxide production, and restored mitochondrial cristae structure.

Endothelial-Specific NOX1 Deletion Abrogates Obesity and Metabolic Syndrome via Preservation of Skeletal Function to Maintain Spontaneous Activity and Exercise Capacity

Because global NOX1 ablation protects mice from high-fat feeding–induced obesity via preservation of mitochondrial function to maintain spontaneous activity and exercise capacity as described above, we further examined the specific role of endothelial NOX1 in this response. Because Cdh5Cre-NOX1CKO and Cdh5Cre-WT mice had similar food and water intake under high-fat feeding (Figure 5A and 5B), we compared spontaneous activity and exercise capacity between the 2 groups. High-fat feeding markedly reduced spontaneous activity in WT littermates, which was restored to near baseline in Cdh5Cre-NOX1CKO mice (Figure 5C), indicating robust protective effects of endothelial NOX1 deletion in preserving spontaneous activity to maintain normal energy expenditure during high-fat feeding. Data indicate that compared with high-fat–fed WT littermates, high-fat–fed Cdh5Cre-NOX1CKO mice also had preserved exercise capacity, reflected by significantly longer exhaustion time, longer traveled distance, and higher exhaustion speed (Figure 5D through 5F, respectively). Besides, oxygen consumption (Figure 5G and 5H) and carbon dioxide production (Figure 5I and 5J) were both significantly enhanced in high-fat–fed Cdh5Cre-NOX1CKO mice compared with Cdh5Cre-WT littermates. These data indicate that endothelial NOX1 knockout restores energy expenditure via preserved spontaneous activity and exercise capacity to protect from high-fat feeding–induced obesity and metabolic syndrome.

Skeletal mitochondrial functions were examined next to validate the elucidated mechanisms, if similar in NOX1 global knockout mice. Transmission electron microscopy results revealed that the density and structure of mitochondrial cristae in soleus muscle Cdh5Cre-NOX1CKO were fully restored compared with high-fat–fed Cdh5Cre-WT littermates (Figure 5K). Besides, the significant increase in calcium-induced mitochondrial swelling induced by high-fat feeding in Cdh5Cre-WT littermates was completely attenuated in Cdh5Cre-NOX1CKO mice (Figure 5L), indicating protected mitochondrial integrity by endothelial-specific NOX1 deletion. In addition, increased mitochondrial superoxide production in skeletal muscle of high-fat–fed Cdh5Cre-WT littermates was significantly alleviated in high-fat–fed Cdh5Cre-NOX1CKO mice (Figure 5M). Therefore, endothelial-specific NOX1 deletion protects against high-fat feeding–induced obesity via preservation of skeletal muscle mitochondrial function to maintain efficient energy expenditure.

Smooth Muscle–Specific NOX1 Deletion Has No Effect on Skeletal Function and Exercise Capacity in Response to High-Fat Feeding

In addition to phenotype analyses for obesity and metabolic syndrome in high-fat–fed Myh11Cre-NOX1CKO mice as described above, we also examined changes in skeletal function and exercise capacity in these animals under high-fat feeding. As shown in Figure S7A through S7C, data from treadmill exercise indicate that Myh11Cre-NOX1CKO and Myh11Cre-WT littermates had similar exhaustion time, distance traveled, and exhaustion speed under high-fat feeding. In addition,

Figure 4 Continued. mitochondria. For **A**, **B**, and **L**, overall effects were assessed by 2-way repeated-measures ANOVA, and differences at individual time points were evaluated using 2-way ANOVA with the Tukey post hoc testing. **C** and **F** were analyzed using 2-way ANOVA with the Tukey post hoc test. **G** through **J** were analyzed using the Mann-Whitney *U* test for daytime and nighttime. **D**, **E**, and **K** were analyzed using 2-way ANOVA with the Newman-Keuls post hoc test. **N** was analyzed using the Mann-Whitney *U* test. Data are shown as mean±SEM. All of the specific *P* values have been included in each graph figure.

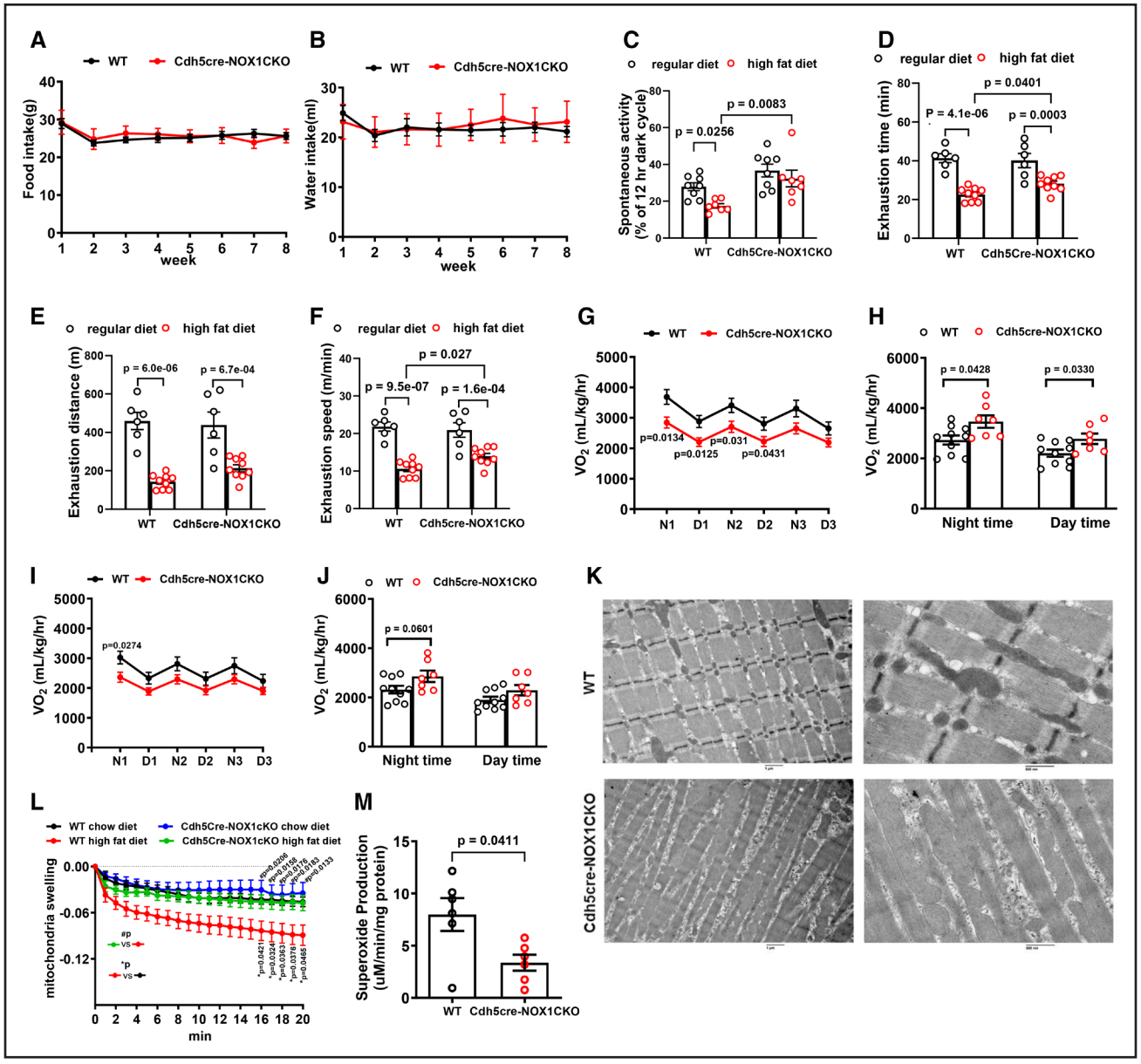

Figure 5. Endothelial-specific NOX1 (NADPH oxidase isoform 1) deletion improved spontaneous activity and exercise capacity via preservation of skeletal mitochondrial function under high-fat feeding.

A, Grouped data of food intake in Cdh5Cre (cadherin 5 [vascular endothelial cadherin] promoter–driven Cre recombinase [endothelial-specific Cre expression])-wild-type (WT) and Cdh5Cre-NOX1CKO mice, indicating similar food intake between the 2 groups in response to a high-fat diet. n=13 for WT; n=4 for Cdh5Cre-NOX1CKO. **B**, Grouped data of water intake in Cdh5Cre-WT and Cdh5Cre-NOX1CKO mice, indicating similar water intake between the 2 groups in response to a high-fat diet. n=13 for WT; n=4 for Cdh5Cre-NOX1CKO. **C**, Mouse spontaneous activity data indicating significantly reduced nighttime activity in high-fat–fed Cdh5Cre-WT mice, which was markedly restored in Cdh5Cre-NOX1CKO mice. n=8 for the WT regular diet group; n=8 for the Cdh5Cre-NOX1CKO regular diet group; n=7 for the WT high-fat-diet group; and n=7 for the Cdh5Cre-NOX1CKO high-fat-diet group. Mouse spontaneous activity was analyzed by a video monitoring system as we previously published. In additional experiments, regular diet–fed and high-fat–fed mice were assayed for exercise capacity using a mouse treadmill system. Exercise capacity was assessed by determining (**D**) exhaustion time, (**E**) total distance traveled at exhaustion, and (**F**) speed at exhaustion. By all 3 parameters, the exercise capacity was found to be markedly decreased in high-fat–fed Cdh5Cre-WT mice, while it was substantially restored in Cdh5Cre-NOX1CKO mice. n=6 for the WT regular diet group; n=6 for the Cdh5Cre-NOX1CKO regular diet group; n=9 for the WT high-fat-diet group; and n=9 for the Cdh5Cre-NOX1CKO high-fat-diet group. **G**, Oxygen consumption data indicating preserved oxygen consumption in high-fat–fed Cdh5Cre-NOX1CKO, which varied normally with circadian rhythm. n=7 for WT; n=10 for Cdh5Cre-NOX1CKO. Oxygen consumption was measured using an Oxymax Comprehensive Lab Animal Monitoring System. **H**, Oxygen consumption during both nighttime and daytime was significantly improved in Cdh5Cre-NOX1CKO mice fed a high-fat diet. *P<0.05 compared with high-fat–fed Cdh5Cre-WT. n=7 for WT; n=10 for Cdh5Cre-NOX1CKO. **I**, CO_2 production data indicating preserved levels of CO_2 production in high-fat–fed Cdh5Cre-NOX1CKO mice, which varied normally with circadian rhythm. *P<0.05 compared with high-fat–fed Cdh5Cre-WT. n=7 for WT; n=10 for Cdh5Cre-NOX1CKO. CO_2 production was measured using an Oxymax Comprehensive Lab Animal Monitoring System. **J**, CO_2 production during both nighttime and daytime was significantly improved in high-fat–fed Cdh5Cre-NOX1CKO mice compared with WT controls. n=7 for WT; n=10 for (*Continued*)

calcium-induced mitochondrial swelling and mitochondrial superoxide production were not affected in high-fat–fed Myh11Cre-NOX1CKO mice compared with high-fat–fed Myh11Cre-WT littermates (Figure S7D and S7E).

Therefore, endothelial NOX1, rather than smooth muscle NOX1, plays a critical intermediate role in high-fat-diet–induced obesity and metabolic syndrome, knockout of which protected against the phenotypes via preservation of skeletal mitochondrial function to maintain spontaneous activity and exercise capacity for sufficient energy expenditure.

Endothelial-Specific NOX1 Transgenesis Worsens Obesity via Deterioration of Skeletal Dysfunction to Impair Exercise Capacity

In further experiments, we also examined exercise capacity and skeletal mitochondrial function in endothelial-specific NOX1 knockin mice. As shown in Figure 6A and 6B, Cdh5Cre-NOX1CKI and Cdh5Cre-WT mice had similar food and water intake. With treadmill training, high-fat–fed Cdh5Cre-NOX1CKI mice displayed significantly shorter exhaustion time, shorter traveled distance, and lower exhaustion speed compared with high-fat–fed Cdh5Cre-WT littermates (Figure 6C through 6E, respectively). In addition, mitochondrial swelling in the skeletal muscle of Cdh5Cre-NOX1CKI mice was deteriorated compared with WT littermates after high-fat feeding (Figure 6F), indicating worsened mitochondrial integrity by overexpression of endothelial NOX1. Transmission electron microscopy results showed lower density and disrupted structure of mitochondrial cristae in Cdh5Cre-NOX1CKI compared with Cdh5Cre-WT mice under high-fat feeding (Figure 6G). Skeletal muscle mitochondrial superoxide production was also significantly increased in high-fat–fed Cdh5Cre-NOX1CKI mice compared with high-fat–fed Cdh5Cre-WT littermates (Figure 6H). Therefore, overexpression of NOX1 specifically in the endothelium deteriorated exercise incapacity and skeletal mitochondrial dysfunction to further worsen phenotypes of obesity and metabolic syndrome.

Restoration of Endothelium-Dependent Vasorelaxation in High-Fat Fed Global and Endothelial-Specific NOX1 Knockout Mice

Endothelium-dependent vasorelaxation was assessed as we previously reported.[34,37] Importantly, the impaired endothelium-dependent vasorelaxation in high-fat–fed WT mice was completely restored in both global NOX1 knockout mice (Figure S8A) and endothelial-specific NOX1 knockout mice (Figure S8B), confirming improvement in endothelial function in these animals under high-fat diet feeding. This supports the hypothesis that endothelial-specific knockdown of NOX1 exerts protective effects on obesity and metabolic syndrome via initial preservation of endothelial function and subsequent protection of adjacent skeletal muscle mitochondrial function, resulting in restored spontaneous and exercise activities to facilitate energy expenditure.

Novel Genetic Signatures in High-Fat Fed Endothelial-Specific NOX1 Knockout Mice Relevant to Skeletal Muscle Function: Cntnap4 and Col9a1

An RNA-sequencing experiment was performed to elucidate potential targets of endothelial-specific activation of NOX1 in modulating skeletal muscle function to result in obesity and metabolic syndrome. The data indicate that 1912 RNA species were upregulated > 2-fold in the soleus muscle of WT mice under high-fat feeding (group 3) compared with WT mice with a regular diet (group 1), among which 667 were protein-coding RNAs (Figure 7A). Among the 667 differentially expressed genes, 408 were downregulated >1.5-fold in Cdh5Cre-NOX1CKO mice under high-fat feeding (group 4) compared with WT littermates under high-fat feeding (group 3; Figure 7B), and 23 protein-coding RNAs were further screened out by significant differences ($P<0.05$) between group 3 and group 1 (Figure 7B and 7C). In addition, 4 protein-coding RNAs were significantly downregulated ($P<0.05$) in group 4 compared with group 3 among the 23 protein-coding RNAs (Figure 7B and 7D).

Figure 5 Continued. Cdh5Cre-NOX1CKO. **K**, Representative images of mitochondria in soleus muscle examined by electron microscopy (EM) at resolution of ×2900 and ×7200, indicating disorganization of mitochondrial cristae in Cdh5Cre-WT mice and complete reversal in Cdh5Cre-NOX1CKO mice, both under high-fat feeding. EM was used to examine mitochondrial cristae structures. **L**, Skeletal mitochondrial data indicating completely reversed swelling activity in Cdh5Cre-NOX1CKO mice fed a high-fat diet compared with high-fat–fed Cdh5Cre-WT mice. n=7 for the WT regular diet group; n=9 for the Cdh5Cre-NOX1CKO regular diet group; n=8 for the WT high-fat-diet group; and n=8 for the Cdh5Cre-NOX1CKO high-fat-diet group. Fresh mitochondria were isolated from skeletal muscle, and mitochondrial swelling was measured by monitoring the decrease in absorbance at 540 nm upon calcium stimulation. **M**, Superoxide production indicating substantially diminished mitochondrial superoxide production in skeletal muscle mitochondrial preparation in high-fat–fed Cdh5Cre-NOX1CKO mice compared with high-fat–fed Cdh5Cre-WT mice. n=6 per group. An electron spin resonance (ESR) spectrophotometer was used to detect superoxide production from freshly prepared skeletal muscle mitochondria. **A** and **B** were assessed by a mixed-effects model (restricted maximum likelihood [REML]) with the Bonferroni multiple comparisons test. For **L**, overall effects were assessed by 2-way repeated-measures ANOVA, and differences at individual time points were evaluated using 2-way ANOVA with the Tukey or Newman-Keuls post hoc testing. **G** through **J** were analyzed using an unpaired *t* test for daytime and nighttime. **C**, **D**, and **F** were analyzed using 2-way ANOVA with the Newman-Keuls post hoc test. **E** was analyzed using 2-way ANOVA with the Tukey post hoc test. **M** was analyzed using the Mann-Whitney *U* test. Data are shown as mean±SEM. All of the specific *P* values have been included in each graph figure.

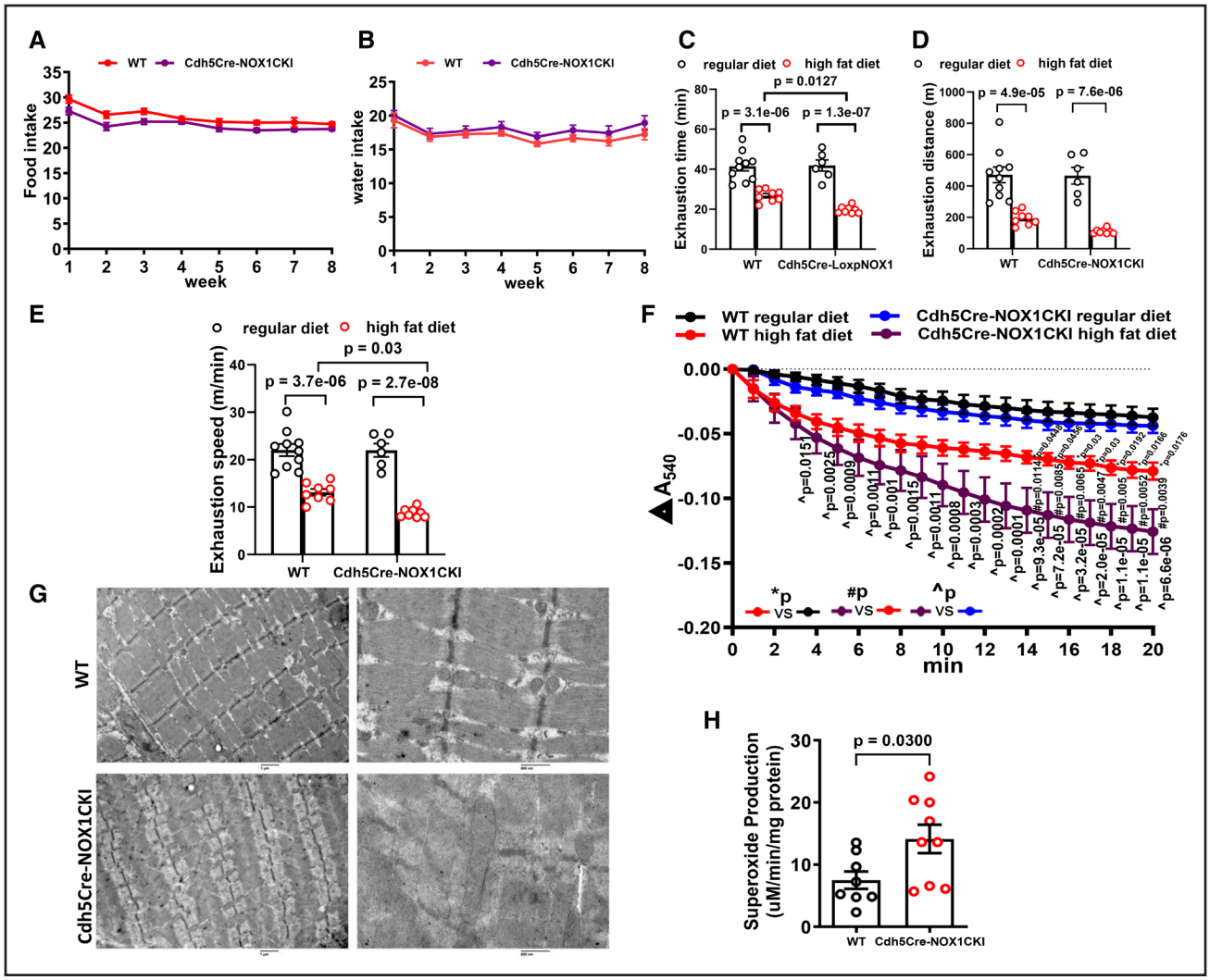

Figure 6. Endothelial-specific NOX1 (NADPH oxidase isoform 1) transgenesis further impaired exercise capacity via deteriorating skeletal mitochondrial function under high-fat feeding.

A, Grouped data of food intake in Cdh5Cre (cadherin 5 [vascular endothelial cadherin] promoter–driven Cre recombinase [endothelial-specific Cre expression])-wild-type (WT) and Cdh5Cre-NOX1CKI mice, indicating similar food intake between the 2 groups in response to a high-fat diet. n=8 for WT; n=11 for Cdh5Cre-NOX1CKI. **B**, Grouped data of water intake in Cdh5Cre-WT and Cdh5Cre-NOX1CKI mice, indicating similar water intake between the 2 groups in response to a high-fat diet. n=8 for WT; n=10 for Cdh5Cre-NOX1CKI. In additional experiments, regular diet–fed and high-fat–fed Cdh5Cre-WT and Cdh5Cre-NOX1CKI mice were assayed for exercise capacity using a mouse treadmill system. Exercise capacity was assessed by determining (**C**) exhaustion time, (**D**) total distance traveled at exhaustion, and (**E**) speed at exhaustion. By all 3 parameters, the exercise capacity was found to be markedly decreased in high-fat–fed Cdh5Cre-WT mice, which was substantially further deteriorated in high-fat–fed Cdh5Cre-NOX1CKI mice. n=10 for the WT regular diet group; n=6 for the Cdh5Cre-cre-inducible NOX1$^{flox/flox}$ knockout/floxed mice (NOX1CKO) regular diet group; n=8 for the WT high-fat-diet group; and n=8 for the Cdh5Cre-NOX1CKO high-fat-diet group. **F**, Skeletal mitochondrial swelling activity was significantly increased in high-fat–fed Cdh5Cre-WT mice, which was substantially further deteriorated in high-fat–fed Cdh5Cre-NOX1CKI mice. Fresh mitochondria were isolated from skeletal muscle, and mitochondrial swelling was measured by monitoring the decrease in absorbance at 540 nm upon calcium stimulation. n=10 for the WT regular diet group; n=9 for the Cdh5Cre-NOX1CKO regular diet group; n=7 for the WT high-fat-diet group; and n=8 for the Cdh5Cre-NOX1CKO high-fat-diet group. **G**, Representative images of mitochondria in soleus muscle examined by electron microscopy (EM) at resolution of ×2900 and ×7200, indicating disorganization of mitochondrial cristae in high-fat–fed Cdh5Cre-WT mice, which was substantially further deteriorated in high-fat–fed Cdh5Cre-NOX1CKI mice. EM was used to examine mitochondrial cristae structures. **H**, Superoxide production data indicating markedly elevated superoxide production in skeletal muscle mitochondrial preparation from high-fat–fed Cdh5Cre-NOX1CKI mice compared with high-fat–fed Cdh5Cre-WT mice. n=8 for WT; n=10 for Cdh5Cre-NOX1CKI. An electron spin resonance (ESR) spectrophotometer was used to detect superoxide production from freshly prepared skeletal muscle mitochondria. For **A**, **B**, and **F**, overall effects were assessed by 2-way repeated-measures ANOVA, and differences at individual time points were evaluated using 2-way ANOVA with the Tukey or Newman-Keuls post hoc testing. **C** through **E** were analyzed using 2-way ANOVA with the Newman-Keuls post hoc test. **H** was analyzed using the unpaired *t* test. Data are shown as mean±SEM. All of the specific *P* values have been included in each graph figure.

ORIGINAL RESEARCH

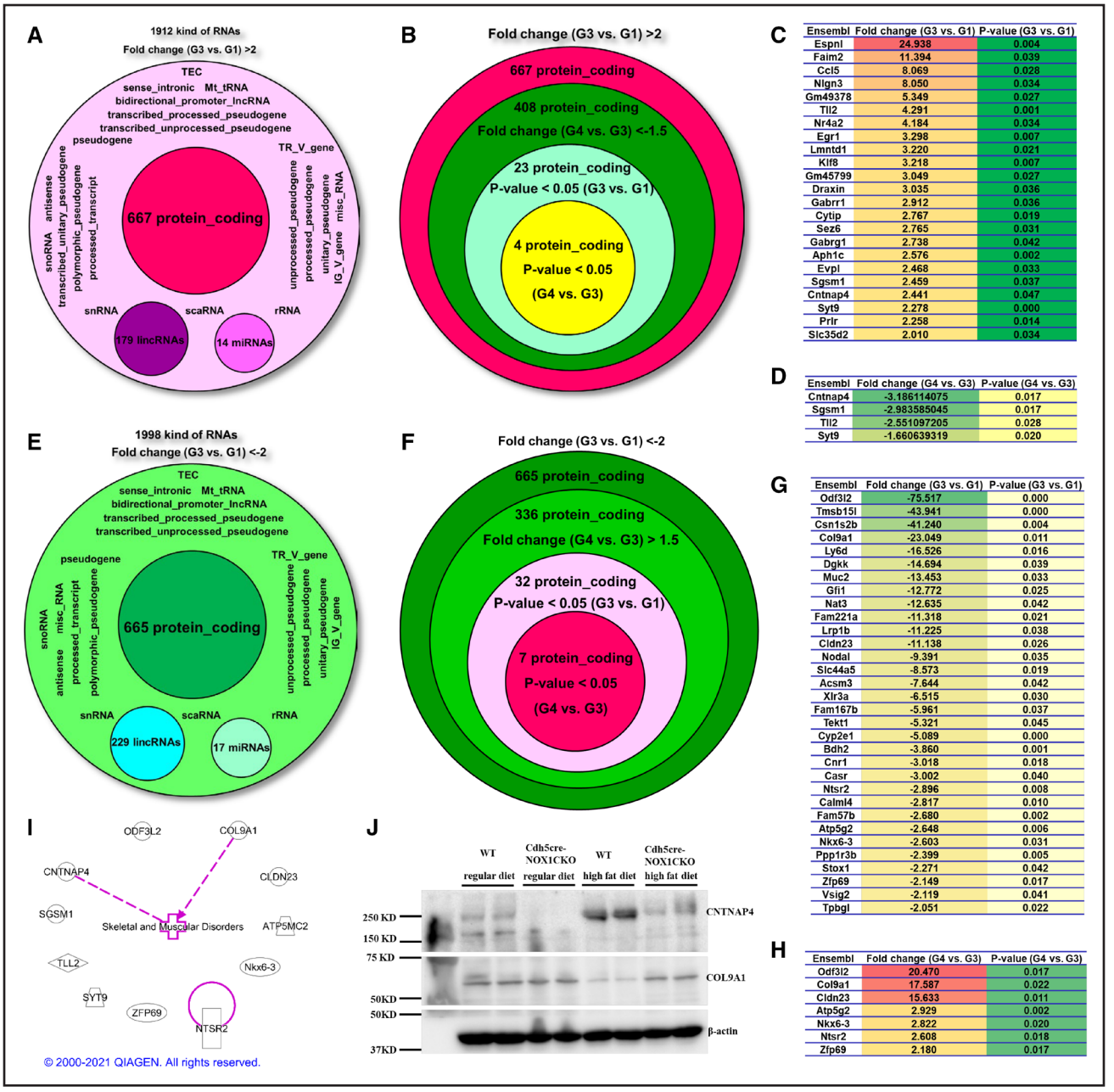

Figure 7. Novel genetic signatures in endothelial-specific NOX1 (NADPH oxidase isoform 1) knockout mice that are linked to modulation of muscular function: Cntnap4 (contactin-associated protein-like 4) and Col9a1 (collagen type IX alpha 1 chain). Soleus muscle samples were prepared from 4 experimental groups of regular diet–fed wild-type (WT) mice (group 1), regular diet–fed Cdh5Cre (cadherin 5 [vascular endothelial cadherin] promoter–driven Cre recombinase [endothelial-specific Cre expression])-cre-inducible NOX1$^{flox/flox}$ knockout/floxed mice (Cdh5Cre-NOX1CKO; group 2), high-fat–fed WT mice (group 3) and high-fat–fed Cdh5Cre-NOX1CKO mice (group 4), and RNA extracted and subjected to RNA-sequencing analysis (n=3 for each group). **A**, Upregulated RNAs (>2-fold) identified from group 3 comparison to group 1, including coding RNAs and noncoding regulatory RNAs. **B**, The screening process to identify protein-coding genes that were significantly upregulated in group 3 compared with group 1 while, at the same time, significantly downregulated in group 4 compared with group 3. **C**, The list of genes that were significantly upregulated in group 3 compared with group 1. **D**, The list of genes that were significantly downregulated in group 4 compared with group 3. **E**, Downregulated RNAs (>2-fold) identified from group 3 comparison to group 1, including coding RNAs and noncoding regulatory RNAs. **F**, The screening process to identify protein-coding genes that were significantly downregulated in group 3 compared with group 1 while, at the same time, significantly upregulated in group 4 compared with group 3. **G**, The list of genes that were significantly downregulated compared with group 3. **H**, The list of genes that were significantly upregulated in group 4 compared with group 3. **I**, The predicted interrelationship between the screened-out genes, and skeletal and muscular disorders analyzed by QIAGEN Ingenuity Pathway Analysis (IPA). **J**, Western blotting results of protein expression levels of Cntnap4 and Col9a1 in soleus muscles of chew diet–fed or high-fat-diet–fed Cdh5cre-WT and Cdh5cre-NOX1CKO mice, confirming similar trends of regulations as identified by RNA-sequencing analysis.

On the other hand, 1998 RNA species were downregulated >2-folds in group 3 compared with group 1, and 665 were protein-coding RNAs among them (Figure 7E). Out of these 665 differentially expressed genes, 336 protein-coding RNAs were increased >1.5-fold in group 4 compared with group 3 (Figure 7F), and 32 protein-coding RNAs were filtered out according to significant differences ($P<0.05$) between group 3 and group 1 (Figure 7F and 7G). Furthermore, 7 protein-coding RNAs were significantly upregulated ($P<0.05$) in group 4 compared with group 3 among the 32 protein-coding RNAs (Figure 7F and 7H).

Next, QIAGEN IPA was used to explore the relationship between the modulated genes in the soleus muscle of Cdh5Cre-NOX1CKO mice and the function of skeletal and muscular disorders. Among the 4 downregulated genes (group 4 versus group 3) and 7 upregulated genes (group 4 versus group 3) screened out by 4 consecutive steps of comparison as described above, only Cntnap4 and Col9a1 were found to connect to the function of skeletal and muscular disorders (Figure 7I). Results of Western blotting analyses confirmed that Cntnap4 was increased by high-fat feeding while decreased by endothelial NOX1 knockout, and Col9a1 was upregulated by high-fat feeding while downregulated by endothelial NOX1 knockout (Figure 7J).

Therefore, Cntnap4 and Col9a1 in the soleus muscle may represent novel genetic signatures underlying endothelial-specific NOX1 activation-driven development of obesity and metabolic syndrome, via impairment in spontaneous activity and exercise capacity under a high-fat diet.

Upregulation of NOX1 in Coronary Arteries of Human Patients With Obesity

To further validate the translational relevance of our findings, we examined the expression of NOX1 in human coronary artery samples isolated from subjects with obesity and normal controls. Coronary artery samples of a total of 15 human subjects (BMI <25, n=6; BMI >25, n=9) were used for the determination of NOX1 expression. The normal weight group consisted of 6 subjects (age: 35.5±9.17 years) with BMI<25, at 18.8±1.33, while the obese group of 9 patients had BMI>25 at 32.5±1.79 (age: 54.4±4.17 years). The authorization and collection of the samples are described in the Methods section. Freshly isolated coronary arteries were dissected, removed of connective tissue carefully, sectioned for separate storage, and snap-frozen. Sections of the coronary arteries were lysated and subjected to WB analysis for NOX1 expression as described in the Methods section. Importantly, we found that NOX1 protein abundance was significantly increased in the coronary arteries of human patients with obesity. Shown are representative Western blots and grouped quantitative data in Figure 8. One limitation is that we have not been able to isolate EC fractions from these tissue samples to examine NOX1 expression selectively in ECs, which warrants further investigation when additional samples are collected from future cohorts.

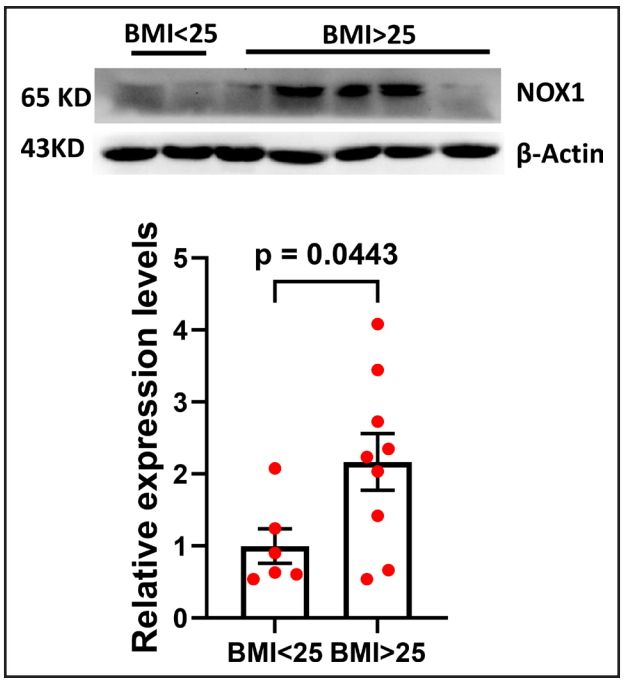

Figure 8. Upregulation of NOX1 (NADPH oxidase isoform 1) in coronary arteries of human patients with obesity. Human patients with obesity and control subjects were enrolled at the Versiti Institute of the Medical College of Wisconsin with approval from the institutional review board at the Medical College of Wisconsin. Specimens from individuals were categorized based on body mass index (BMI). Coronary arteries were dissected and immediately transferred to ice-cold PBS solution to preserve tissue integrity. Connective tissue was carefully removed, and the arteries were divided into sections and snap-frozen. Sections of the coronary arteries were lysated and subjected to Western blotting analysis for NOX1 expression. Shown are representative Western blots and grouped densitometric data indicating marked upregulation of NOX1 in the coronary arteries of human patients with obesity with BMI >25. n=6 for patients with BMI <25; n=9 for patients with BMI >25. Data were analyzed using the unpaired *t* test. Data are shown as mean±SEM. The specific *P* value has been included in the graph.

DISCUSSION

The most significant findings of this study are given as follows: (1) global knockout of NOX1, rather than of NOX2/NOX4, substantially abrogated features of obesity and metabolic syndrome, including increased body weight, fat mass, liver weight, adipocyte differentiation, glucose intolerance, plasma insulin, and leptin levels. (2) endothelial-specific NOX1 deletion, rather than vascular smooth muscle–specific NOX1 deletion, substantially alleviated features of obesity and metabolic syndrome in response to high-fat feeding, establishing a novel, selective, and tissue-specific role of endothelial NOX1

in driving systematic metabolic responses. This is further confirmed by data collected using endothelial-specific NOX1 knockin mice, in which high-fat feeding resulted in exaggerated phenotypes of obesity and metabolic syndrome. (3) Global and EC-specific deletion of NOX1 in mice led to preserved energy expenditure under high-fat feeding via restoration of skeletal muscle mitochondrial function to result in preserved spontaneous activity and exercise capacity, therefore alleviating the development of obesity and metabolic syndrome. This is further validated by data from EC-specific knockin mice in which a high-fat-diet–induced worsened skeletal muscle mitochondrial dysfunction and exercise incapacity. (4) RNA-sequencing analyses identified novel genetic signatures of Cntnap4 and Col9a1 in soleus muscles of endothelial-specific NOX1 knockout mice under a high-fat diet, which are linked to the modulation of skeletal muscle function. (5) NOX1 expression was significantly upregulated in human patients with obesity, indicating robust translational relevance of our findings. These observations are paradigm-shifting in establishing a novel, significant, specific, and selective role of endothelial-specific activation of NOX1 in driving obesity and metabolic syndrome under high-fat feeding, via deficiencies in skeletal muscle mitochondrial function to result in impaired spontaneous activity, exercise capacity, and energy expenditure.

Accumulating evidence has demonstrated that the NOX family of enzymes plays a major role in the pathogenesis of various vascular diseases, such as hypertension, aortic aneurysms, atherosclerosis, and diabetic vascular complications, as well as for the development of cardiac disorders, including ischemia-reperfusion injury, myocardial infarction, heart failure, and cardiac arrhythmias.[11] NOX1, NOX2, or NOX4 lies upstream of DHFR (dihydrofolate reductase) deficiency to induce abdominal aortic aneurysm formation.[21,23] NOX4-induced ROS production mediates development of thoracic aortic aneurysm and abdominal aortic aneurysm in Marfan syndrome mice.[22] NOX4 activation, subsequent ROS production, and redox-sensitive CaMKII (calcium/calmodulin-dependent protein kinase II) activation underlie the pathogenesis of cardiac arrhythmia.[30] Either NOX1 or NOX2, or both, has been shown to be activated in the processes of atherosclerosis,[38] while other studies implicated a protective role of NOX4 in atherosclerosis utilizing different model systems.[39–41] As the only membrane-bound subunit for NOX, $p22^{phox}$ is required for catalytic activation of NOX1 to NOX4,[10,11] and excessive vascular ROS produced by $p22^{phox}$ plays a causal role in obesity by promoting inflammation, adipogenesis, and exercise intolerance.[8] However, the differential roles and related molecular mechanisms of NOX isoforms in the modulation of obesity and metabolic syndrome had remained completely unknown until our present study. High-fat-diet–induced body weight gain, fat mass gain, liver weight gain, preadipocyte differentiation, glucose intolerance, insulin/leptin resistance, and hypercholesterolemia were all substantially alleviated in NOX1 global knockout mice but unaffected in NOX2 or NOX4 global knockout mice. Of note, this protective effect was not derived from changes in energy intake, as WT and NOX1 global knockout mice had similar intake of food and water. On the other hand, high-fat feeding–induced impairment in spontaneous activity, exercise capacity, respiratory performance, and skeletal muscle mitochondrial function were all markedly abrogated in NOX1 global knockout mice to result in improved ATP production and energy expenditure. In addition, endothelium-dependent vasorelaxation was also fully restored in global and endothelial-specific NOX1 knockout mice, confirming improvement in endothelial function as the initiating factor of the protective signaling. Taken together with our earlier observations that vascular $p22^{phox}$-dependent NOX drives development of obesity and metabolic syndrome, our data at first verified that vascular NOX1 rather than NOX2 or NOX4 is the source of vascular oxidative stress that is acting as a driving force to induce phenotypes of obesity and metabolic syndrome under high-fat feeding. These findings further establish the paradigm-shifting concept that vascular-derived oxidative stress from activated NOX1 is a cause of obesity and metabolic syndrome rather than a consequence.

Oxidative stress has been shown to impair skeletal muscle energy metabolism in mice and human patients.[35,42–46] Angiotensin II–induced oxidative stress causes deficiency in mitochondrial respiration in skeletal muscle of C57BL/6 mice.[44] Systemic oxidative stress has been found to be associated with impaired skeletal muscle energy metabolism in patients with metabolic syndrome or heart failure.[42,43] Our previous work also revealed skeletal muscle mitochondrial dysfunction in mice with vascular ROS overproduction.[8] However, the exact source of ROS and how it impacts skeletal muscle function have remained unclear until our present study. In this work, we elucidated that vascular endothelial NOX1, rather than smooth muscle cell NOX1, produced ROS to damage skeletal muscle mitochondrial function, resulting in impaired spontaneous activity and exercise capacity under high-fat diet. Consistently, endothelial-specific overexpression of NOX1 in mice led to deteriorated skeletal muscle mitochondrial dysfunction in response to high-fat feeding. Besides, mitochondrial ROS production was decreased by endothelial-specific NOX1 knockout while increased by endothelial-specific NOX1 knockin. Of note, blood vessels are closely intertwined with skeletal muscle tissues lying between the fascicles and bundles of muscle fibers. Each muscle is supplied by many capillaries, which contain lots of ECs rather than smooth muscle cells. The increase in bulk muscle blood flow observed during exercise is accompanied by a substantial elevation in capillary recruitment within the muscle that expands the surface area.[47] This close association reduces the diffusion distances, allowing for efficient exchange of oxygen

and nutrients required for contraction and rapid removal of injurious metabolic wastes. Therefore, vascular ROS is capable of diffusing to adjacent skeletal muscle cells to induce mitochondrial dysfunction and mitochondrial ROS production in these cells.

Exercise intolerance and mitochondrial complex I and II deficiencies have been reported in high-fat–fed C57/BL6 mice.[35] Alongside these changes, the respiratory control ratio (RCR), as the single most useful general measure of function in isolated mitochondria,[48] was impaired in high-fat–fed WT mice in our present study but substantially restored by global and endothelial-specific knockout of NOX1. Excessive mitochondrial swelling, representative of impaired mitochondrial integrity that occurs following increased opening of mitochondrial permeability transition pores, is a central player that can induce cell death through apoptosis or necrosis, depending on the availability of ATP.[49] Mitochondrial swelling has been reported in skeletal muscle of mice fed a high-fat diet due to increased ROS production in the muscle.[50] In this study, we found markedly increased mitochondrial swelling by high-fat feeding in WT mice, while global and endothelial-specific deletion of NOX1 completely attenuated this process. However, endothelial-specific NOX1 knockin further increased mitochondrial swelling under high-fat feeding. We also found that high-fat feeding–induced marked increase in mitochondrial ROS production in skeletal muscle was substantially alleviated by global or endothelial-specific knockout of NOX1. By contrast, NOX1-specific overexpression in ECs exaggerated mitochondrial ROS production in skeletal muscle. Taken together, these data indicate that endothelial-specific NOX1 activation induces skeletal muscle mitochondrial dysfunction that is characterized by reduced respiratory performance, increased mitochondrial swelling, and increased mitochondrial ROS production. The mitochondrial electron transport chain is located within mitochondrial cristae where it generates the electrochemical potential across the invaginated inner mitochondrial membranes, which is used for ATP synthesis.[51] Cristae orientation, curvature, and density per surface area are nonrandom, exhibiting directionality and orientation that may enable cristae membranes of adjacent mitochondria to become physically and energetically coordinated.[51] In this work, we revealed that disorganized mitochondrial cristae in WT mice fed a high-fat diet, which was completely abrogated by global or endothelial-specific deletion of NOX1. Of note, we found much lower density and more disrupted structure of mitochondrial cristae in endothelial-specific NOX1 knockin mice. These results showed that endothelial-specific NOX1 activation destroys mitochondrial cristae structure and ATP production. Therefore, endothelial-specific activation of NOX1 impairs skeletal muscle mitochondrial function through a diversity of processes, resulting in impairment in spontaneous activity and exercise capacity to suppress energy expenditure. This conclusion is supported by data from both endothelial-specific knockout and knockin mice.

Global NOX1 knockout mice have been previously studied for their roles in diabetic vascular dysfunction and atherogenesis, as reported by others and our own work.[8,24,52,53] Besides being implicated to mediate diabetic endothelial dysfunction and accelerated atherogenesis,[8,24,52–54] it was reported that NOX1 is involved in the dysfunction of liver sinusoids in nonalcoholic fatty liver disease.[55] These findings seem to share similarity with our previous work establishing a critical role of $p22^{phox}$ in mediating obesity and metabolic syndrome as a catalytic subunit capable of activating NOX1,[8] which was highlighted by an editorial commentary emphasizing a paradigm-shifting novel concept of vascular ROS driving systematic responses of obesity and metabolic syndrome.[56] It would also be critical to further examine detailed mechanistic pathways by which endothelial NOX1 is triggered to initiate the processes of obesity and metabolic dysfunction.

Importantly, the only 2 novel genes of Cntnap4 and Col9a1 were specifically screened out via RNA-sequencing and IPA analysis in this study, which are regulated in the skeletal muscle to be responsible for the changes in function induced by high-fat feeding that was reversed by endothelial-specific deletion of NOX1. Existing studies indicate that Cntnap4 is a member of the neurexin superfamily of transmembrane molecules that have critical functions in neuronal cell communication.[57] It was shown that Cntnap4 plays a critical role in osteogenesis, which is the first functional annotation for Cntnap4 in the musculoskeletal system.[57] Interestingly, recent studies indicate that microRNA-34 uniquely regulates Cntnap4 expression, which may be regulated in obesity to contribute to Cntnap4-dependent modulation of skeletal muscle function.[58] The *Col9a1* gene has been implicated in the initial stages of skeletal muscle cell differentiation and found associated with the longissimus dorsi muscle in the pig.[59] Some of the genetic variants of Col9a1 have been identified.[60] It would be interesting to explore whether these variants are present in human patients with obesity. In this research, we found that Cntnap4 was upregulated, while Col9a1 was downregulated in the skeletal muscle of high-fat–fed WT mice, and endothelial-specific NOX1 ablation reversed these responses, indicating that the regulation of these novel genes likely underlie high-fat feeding–induced skeletal muscle phenotypes that are correctable by deletion of endothelial NOX1. Detailed molecular pathways controlling the regulation of Cntnap4 and Col9a1 in skeletal muscle warrant further investigations.

Importantly, utilizing coronary arteries isolated from human patients with obesity and control subjects, we found that NOX1 protein expression was markedly increased in obese subjects (BMI >25) compared with normal weight controls (BMI <25). This indicates that the sophisticated mechanistic insights we identified for

vascular NOX1-driven development of obesity and metabolic syndrome, are relevant to human subjects with great translational potential. Of note, this regulation we observed is consistent with previous work by Matsumoto at al,[55] reporting upregulated NOX1 mRNA expression in human nonalcoholic steatohepatitis patients.

Of note, our studies were performed primarily using male mice. It would be important to also examine the new pathways and mechanisms in female mice. It was shown that female mitochondria have higher functional capacity and greater resistance to oxidative damage than male mitochondria.[61] Whereas mitochondria might be less injured in obese females, preservation of mitochondrial function might have more sensitive outcomes in reducing obesity and metabolic syndrome. It was proposed that sex steroid hormones and gut microbiota diversity, chromosomal and genetic variables, and behavioral and sociocultural variables all influence obesity development in men and women. It is, therefore, a complex question to address how the endothelial-specific NOX1 activation drives obesity in females differentially, which warrants immediate further studies.[62] Many novel mediators in adipose tissues have been recently revealed,[63,64] and it is also important to understand how they differ between males and females in regulating adipogenesis and obesity.

In conclusion, observations in our present study firmly establish a direct causal role of endothelial-specific activation of NOX1 in driving the development of systematic disorders of obesity and metabolic syndrome. ROS produced from activated NOX1 in the ECs diffuses to adjacent skeletal muscle to induce mitochondrial dysfunction, resulting in impaired spontaneous activity and exercise capacity, and ultimately a severe deficiency in energy expenditure to allow development of obesity and metabolic syndrome. Novel genes of Cntnap4 and Col9a1 in skeletal muscle were identified being relevant to these processes. NOX1 protein expression was indeed upregulated in the coronary arteries of human patients with obesity. Therefore, specific and selective targeting of endothelial NOX1, or Cntmap4/Col9a1 in the skeletal muscle, may prove to be innovatively and robustly effective for the treatment and prevention of obesity and metabolic syndrome.

ARTICLE INFORMATION

Received May 09, 2025; revision received March 25, 2026; accepted March 30, 2026.

Affiliations

Division of Molecular Medicine, Department of Anesthesiology and Perioperative Medicine, Division of Cardiology, Department of Medicine, David Geffen School of Medicine, University of California, Los Angeles (K.H., Y.H., Yuhan Zhang, Yixuan Zhang, N.W.H., H.C.). Department of Anesthesiology, Medical College of Wisconsin, Milwaukee (J.K.F.).

Sources of Funding

This work was supported by the National Institutes of Health, National Heart, Lung, and Blood Institute awards HL142951 (to H. Cai), HL154754 (to H. Cai), and HL162407 (H. Cai).

Disclosures

None.

Supplemental Material

Supplemental Materials and Methods
Figures S1–S6
Major Resources Table
Uncropped Western Blots
References 8, 27, 31, 34

REFERENCES

1. Powell-Wiley TM, Poirier P, Burke LE, Despres JP, Gordon-Larsen P, Lavie CJ, Lear SA, Ndumele CE, Neeland IJ, Sanders P, et al; American Heart Association Council on Lifestyle and Cardiometabolic Health; Council on Cardiovascular and Stroke Nursing; Council on Clinical Cardiology; Council on Epidemiology and Prevention; and Stroke Council. Obesity and cardiovascular disease: a scientific statement from the American Heart Association. *Circulation*. 2021;143:e984–e1010. doi: 10.1161/CIR.0000000000000973
2. Maffetone PB, Rivera-Dominguez I, Laursen PB. Overfat and underfat: new terms and definitions long overdue. *Front Public Health*. 2016;4:279. doi: 10.3389/fpubh.2016.00279
3. Srivastava G, Apovian CM. Current pharmacotherapy for obesity. *Nat Rev Endocrinol*. 2018;14:12–24. doi: 10.1038/nrendo.2017.122
4. Blüher M. Obesity: global epidemiology and pathogenesis. *Nat Rev Endocrinol*. 2019;15(5):288–298. doi: 10.1038/s41574-019-0176-8
5. The Lancet Gastroenterology Hepatology. Obesity: another ongoing pandemic. *Lancet Gastroenterol Hepatol*. 2021;6:411. doi: 10.1016/S2468-1253(21)00143-6
6. Cardel MI, Atkinson MA, Taveras EM, Holm JC, Kelly AS. Obesity treatment among adolescents: a review of current evidence and future directions. *JAMA Pediatr*. 2020;174:609–617. doi: 10.1001/jamapediatrics.2020.0085
7. Cignarella A, Busetto L, Vettor R. Pharmacotherapy of obesity: an update. *Pharmacol Res*. 2021;169:105649. doi: 10.1016/j.phrs.2021.105649
8. Youn JY, Siu KL, Lob HE, Itani H, Harrison DG, Cai H. Role of vascular oxidative stress in obesity and metabolic syndrome. *Diabetes*. 2014;63:2344–2355. doi: 10.2337/db13-0719
9. Forrester SJ, Kikuchi DS, Hernandes MS, Xu Q, Griendling KK. Reactive oxygen species in metabolic and inflammatory signaling. *Circ Res*. 2018;122:877–902. doi: 10.1161/CIRCRESAHA.117.311401
10. Santillo M, Colantuoni A, Mondola P, Guida B, Damiano S. NOX signaling in molecular cardiovascular mechanisms involved in the blood pressure homeostasis. *Front Physiol*. 2015;6:194. doi: 10.3389/fphys.2015.00194
11. Zhang Y, Murugesan P, Huang K, Cai H. NADPH oxidases and oxidase crosstalk in cardiovascular diseases: novel therapeutic targets. *Nat Rev Cardiol*. 2020;17:170–194. doi: 10.1038/s41569-019-0260-8
12. Brandes RP, Schroder K. Differential vascular functions of Nox family NADPH oxidases. *Curr Opin Lipidol*. 2008;19:513–518. doi: 10.1097/MOL.0b013e32830c91e3
13. Ray R, Shah AM. NADPH oxidase and endothelial cell function. *Clin Sci (Lond)*. 2005;109:217–226. doi: 10.1042/CS20050067
14. Cai H, Harrison DG. Endothelial dysfunction in cardiovascular diseases: the role of oxidant stress. *Circ Res*. 2000;87:840–844. doi: 10.1161/01.res.87.10.840
15. Cai H, Griendling KK, Harrison DG. The vascular NAD(P)H oxidases as therapeutic targets in cardiovascular diseases. *Trends Pharmacol Sci*. 2003;24:471–478. doi: 10.1016/S0165-6147(03)00233-5
16. Cai H. Hydrogen peroxide regulation of endothelial function: origins, mechanisms, and consequences. *Cardiovasc Res*. 2005;68:26–36. doi: 10.1016/j.cardiores.2005.06.021
17. Cai H. NAD(P)H oxidase-dependent self-propagation of hydrogen peroxide and vascular disease. *Circ Res*. 2005;96:818–822. doi: 10.1161/01.RES.0000163631.07205.fb
18. Lassegue B, San Martin A, Griendling KK. Biochemistry, physiology, and pathophysiology of NADPH oxidases in the cardiovascular system. *Circ Res*. 2012;110:1364–1390. doi: 10.1161/CIRCRESAHA.111.243972
19. Matsuno K, Yamada H, Iwata K, Jin D, Katsuyama M, Matsuki M, Takai S, Yamanishi K, Miyazaki M, Matsubara H, et al. Nox1 is involved in angiotensin II-mediated hypertension: a study in Nox1-deficient mice. *Circulation*. 2005;112:2677–2685. doi: 10.1161/CIRCULATIONAHA.105.573709
20. Bendall JK, Rinze R, Adlam D, Tatham AL, de Bono J, Wilson N, Volpi E, Channon KM. Endothelial Nox2 overexpression potentiates vascular oxidative stress and hemodynamic response to angiotensin II: studies

in endothelial-targeted Nox2 transgenic mice. *Circ Res*. 2007;100:1016–1025. doi: 10.1161/01.RES.0000263381.83835.7b
21. Siu KL, Li Q, Zhang Y, Guo J, Youn JY, Du J, Cai H. NOX isoforms in the development of abdominal aortic aneurysm. *Redox Biol*. 2017;11:118–125. doi: 10.1016/j.redox.2016.11.002
22. Huang K, Wang Y, Siu KL, Zhang Y, Cai H. Targeting feed-forward signaling of TGFβ/NOX4/DHFR/eNOS uncoupling/TGFβ axis with anti-TGFβ and folic acid attenuates formation of aortic aneurysms: novel mechanisms and therapeutics. *Redox Biol*. 2021;38:101757. doi: 10.1016/j.redox.2020.101757
23. Huang K, Narumi T, Zhang Y, Li Q, Murugesan P, Wu Y, Liu NM, Cai H. Targeting MicroRNA-192-5p, a downstream effector of NOXs (NADPH oxidases), reverses endothelial DHFR (dihydrofolate reductase) deficiency to attenuate abdominal aortic aneurysm formation. *Hypertension*. 2021;78:282–293. doi: 10.1161/HYPERTENSIONAHA.120.15070
24. Youn JY, Gao L, Cai H. The p47phox- and NADPH oxidase organiser 1 (NOXO1)-dependent activation of NADPH oxidase 1 (NOX1) mediates endothelial nitric oxide synthase (eNOS) uncoupling and endothelial dysfunction in a streptozotocin-induced murine model of diabetes. *Diabetologia*. 2012;55:2069–2079. doi: 10.1007/s00125-012-2557-6
25. Oak JH, Cai H. Attenuation of angiotensin II signaling recouples eNOS and inhibits nonendothelial NOX activity in diabetic mice. *Diabetes*. 2007;56:118–126. doi: 10.2337/db06-0288
26. Youn JY, Zhou J, Cai H. Bone Morphogenic protein 4 mediates NOX1-dependent eNOS uncoupling, endothelial dysfunction, and COX2 induction in type 2 diabetes mellitus. *Mol Endocrinol*. 2015;29:1123–1133. doi: 10.1210/ME.2014-1313
27. Siu KL, Lotz C, Ping P, Cai H. Netrin-1 abrogates ischemia/reperfusion-induced cardiac mitochondrial dysfunction via nitric oxide-dependent attenuation of NOX4 activation and recoupling of NOS. *J Mol Cell Cardiol*. 2015;78:174–185. doi: 10.1016/j.yjmcc.2014.07.005
28. Matsushima S, Kuroda J, Ago T, Zhai P, Ikeda Y, Oka S, Fong GH, Tian R, Sadoshima J. Broad suppression of NADPH oxidase activity exacerbates ischemia/reperfusion injury through inadvertent downregulation of hypoxia-inducible factor-1α and upregulation of peroxisome proliferator-activated receptor-α. *Circ Res*. 2013;112:1135–1149. doi: 10.1161/CIRCRESAHA.111.300171
29. Zhang J, Youn JY, Kim AY, Ramirez RJ, Gao L, Ngo D, Chen P, Scovotti J, Mahajan A, Cai H. NOX4-dependent hydrogen peroxide overproduction in human atrial fibrillation and HL-1 atrial cells: relationship to hypertension. *Front Physiol*. 2012;3:140. doi: 10.3389/fphys.2012.00140
30. Zhang Y, Shimizu H, Siu KL, Mahajan A, Chen JN, Cai H. NADPH oxidase 4 induces cardiac arrhythmic phenotype in zebrafish. *J Biol Chem*. 2014;289:23200–23208. doi: 10.1074/jbc.M114.587196
31. Wang Y, Nakayama M, Pitulescu ME, Schmidt TS, Bochenek ML, Sakakibara A, Adams S, Davy A, Deutsch U, Luthi U, et al. Ephrin-B2 controls VEGF-induced angiogenesis and lymphangiogenesis. *Nature*. 2010;465:483–486. doi: 10.1038/nature09002
32. Monvoisin A, Alva JA, Hofmann JJ, Zovein AC, Lane TF, Iruela-Arispe ML. VE-cadherin-CreERT2 transgenic mouse: a model for inducible recombination in the endothelium. *Dev Dyn*. 2006;235:3413–3422. doi: 10.1002/dvdy.20982
33. Wirth A, Benyo Z, Lukasova M, Leutgeb B, Wettschureck N, Gorbey S, Orsy P, Horvath B, Maser-Gluth C, Greiner E, et al. G12-G13-LARG-mediated signaling in vascular smooth muscle is required for salt-induced hypertension. *Nat Med*. 2008;14:64–68. doi: 10.1038/nm1666
34. Guo Z, Zhang Y, Liu C, Youn JY, Cai HL. Toll-like receptor 2 (TLR2) knockout abrogates diabetic and obese phenotypes while restoring endothelial function via inhibition of NOX1. *Diabetes*. 2021;70:2107–2119. doi: 10.2337/db20-0591
35. Yokota T, Kinugawa S, Hirabayashi K, Matsushima S, Inoue N, Ohta Y, Hamaguchi S, Sobirin MA, Ono T, Suga T, et al. Oxidative stress in skeletal muscle impairs mitochondrial respiration and limits exercise capacity in type 2 diabetic mice. *Am J Physiol Heart Circ Physiol*. 2009;297:H1069–H1077. doi: 10.1152/ajpheart.00267.2009
36. Cogliati S, Enriquez JA, Scorrano L. Mitochondrial cristae: where beauty meets functionality. *Trends Biochem Sci*. 2016;41:261–273. doi: 10.1016/j.tibs.2016.01.001
37. Youn JY, Wang T, Blair J, Laude KM, Oak JH, McCann LA, Harrison DG, Cai H. Endothelium-specific sepiapterin reductase deficiency in DOCA-salt hypertension. *Am J Physiol Heart Circ Physiol*. 2012;302:H2243–H2249. doi: 10.1152/ajpheart.00835.2011
38. Barry-Lane PA, Patterson C, van der Merwe M, Hu Z, Holland SM, Yeh ET, Runge MS. p47phox is required for atherosclerotic lesion progression in ApoE(-/-) mice. *J Clin Invest*. 2001;108:1513–1522. doi: 10.1172/JCI11927
39. Schurmann C, Rezende F, Kruse C, Yasar Y, Lowe O, Fork C, van de Sluis B, Bremer R, Weissmann N, Shah AM, et al. The NADPH oxidase Nox4 has anti-atherosclerotic functions. *Eur Heart J*. 2015;36:3447–3456. doi: 10.1093/eurheartj/ehv460
40. Langbein H, Brunssen C, Hofmann A, Cimalla P, Brux M, Bornstein SR, Deussen A, Koch E, Morawietz H. NADPH oxidase 4 protects against development of endothelial dysfunction and atherosclerosis in LDL receptor deficient mice. *Eur Heart J*. 2016;37:1753–1761. doi: 10.1093/eurheartj/ehv564
41. Gray SP, Di Marco E, Kennedy K, Chew P, Okabe J, El-Osta A, Calkin AC, Biessen EA, Touyz RM, Cooper ME, et al. Reactive oxygen species can provide atheroprotection via NOX4-dependent inhibition of inflammation and vascular remodeling. *Arterioscler Thromb Vasc Biol*. 2016;36:295–307. doi: 10.1161/ATVBAHA.115.307012
42. Yokota T, Kinugawa S, Yamato M, Hirabayashi K, Suga T, Takada S, Harada K, Morita N, Oyama-Manabe N, Kikuchi Y, et al. Systemic oxidative stress is associated with lower aerobic capacity and impaired skeletal muscle energy metabolism in patients with metabolic syndrome. *Diabetes Care*. 2013;36:1341–1346. doi: 10.2337/dc12-1161
43. Yokota T, Kinugawa S, Hirabayashi K, Yamato M, Takada S, Suga T, Nakano I, Fukushima A, Matsushima S, Okita K, et al. Systemic oxidative stress is associated with lower aerobic capacity and impaired skeletal muscle energy metabolism in heart failure patients. *Sci Rep*. 2021;11:2272. doi: 10.1038/s41598-021-81736-0
44. Inoue N, Kinugawa S, Suga T, Yokota T, Hirabayashi K, Kuroda S, Okita K, Tsutsui H. Angiotensin II-induced reduction in exercise capacity is associated with increased oxidative stress in skeletal muscle. *Am J Physiol Heart Circ Physiol*. 2012;302:H1202–H1210. doi: 10.1152/ajpheart.00534.2011
45. Kinugawa S, Wang Z, Kaminski PM, Wolin MS, Edwards JG, Kaley G, Hintze TH. Limited exercise capacity in heterozygous manganese superoxide dismutase gene-knockout mice: roles of superoxide anion and nitric oxide. *Circulation*. 2005;111:1480–1486. doi: 10.1161/01.CIR.0000159261.11520.63
46. Kuwahara H, Horie T, Ishikawa S, Tsuda C, Kawakami S, Noda Y, Kaneko T, Tahara S, Tachibana T, Okabe M, et al. Oxidative stress in skeletal muscle causes severe disturbance of exercise activity without muscle atrophy. *Free Radic Biol Med*. 2010;48:1252–1262. doi: 10.1016/j.freeradbiomed.2010.02.011
47. Sylow L, Kleinert M, Richter EA, Jensen TE. Exercise-stimulated glucose uptake - regulation and implications for glycaemic control. *Nat Rev Endocrinol*. 2017;13:133–148. doi: 10.1038/nrendo.2016.162
48. Brand MD, Nicholls DG. Assessing mitochondrial dysfunction in cells. *Biochem J*. 2011;435:297–312. doi: 10.1042/BJ20110162
49. Javadov S, Chapa-Dubocq X, Makarov V. Different approaches to modeling analysis of mitochondrial swelling. *Mitochondrion*. 2018;38:58–70. doi: 10.1016/j.mito.2017.08.004
50. Bonnard C, Durand A, Peyrol S, Chanseaume E, Chauvin MA, Morio B, Vidal H, Rieusset J. Mitochondrial dysfunction results from oxidative stress in the skeletal muscle of diet-induced insulin-resistant mice. *J Clin Invest*. 2008;118:789–800. doi: 10.1172/JCI32601
51. Picard M, McManus MJ, Csordas G, Varnai P, Dorn GW 2nd, Williams D, Hajnoczky G, Wallace DC. Trans-mitochondrial coordination of cristae at regulated membrane junctions. *Nat Commun*. 2015;6:6259. doi: 10.1038/ncomms7259
52. Sobey CG, Judkins CP, Rivera J, Lewis CV, Diep H, Lee HW, Kemp-Harper BK, Broughton BR, Selemidis S, Gaspari TA, et al. NOX1 deficiency in apolipoprotein E-knockout mice is associated with elevated plasma lipids and enhanced atherosclerosis. *Free Radic Res*. 2015;49:186–198. doi: 10.3109/10715762.2014.992893
53. Zhang Y, Youn JY, Huang K, Zhang Y, Cai H. Alleviation of accelerated diabetic atherogenesis in STZ-treated apoE/NOX1 DKO mice, apoE-/-/tg-EC-DHFR mice, and by folic acid. *Redox Biol*. 2025;82:103570. doi: 10.1016/j.redox.2025.103570
54. Sheehan AL, Carrell S, Johnson B, Stanic B, Banfi B, Miller FJ Jr. Role for Nox1 NADPH oxidase in atherosclerosis. *Atherosclerosis*. 2011;216:321–326. doi: 10.1016/j.atherosclerosis.2011.02.028
55. Matsumoto M, Zhang J, Zhang X, Liu J, Jiang JX, Yamaguchi K, Taruno A, Katsuyama M, Iwata K, Ibi M, et al. The NOX1 isoform of NADPH oxidase is involved in dysfunction of liver sinusoids in nonalcoholic fatty liver disease. *Free Radic Biol Med*. 2018;115:412–420. doi: 10.1016/j.freeradbiomed.2017.12.019
56. Aroor AR, DeMarco VG. Oxidative stress and obesity: the chicken or the egg? *Diabetes*. 2014;63:2216–2218. doi: 10.2337/db14-0424
57. Li C, Zheng Z, Ha P, Chen X, Jiang W, Sun S, Chen F, Asatrian G, Berthiaume EA, Kim JK, et al. Neurexin superfamily cell membrane receptor contactin-associated protein like-4 (Cntnap4) is involved in neural EGFL-like

1 (Nell-1)-responsive osteogenesis. *J Bone Miner Res*. 2018;33:1813–1825. doi: 10.1002/jbmr.3524
58. McNeill EM, Warinner C, Alkins S, Taylor A, Heggeness H, DeLuca TF, Fulga TA, Wall DP, Griffith LC, Van Vactor D. The conserved microRNA miR-34 regulates synaptogenesis via coordination of distinct mechanisms in presynaptic and postsynaptic cells. *Nat Commun*. 2020;11:1092. doi: 10.1038/s41467-020-14761-8
59. Fan B, Onteru SK, Nikkila MT, Stalder KJ, Rothschild MF. The COL9A1 gene is associated with longissimus dorsi muscle area in the pig. *Anim Genet*. 2009;40:788. doi: 10.1111/j.1365-2052.2009.01885.x
60. Hofrichter MAH, Doll J, Habibi H, Enayati S, Vahidi Mehrjardi MY, Müller T, Dittrich M, Haaf T, Vona B. Exome-wide copy number variation analysis identifies a COL9A1 in frame deletion that is associated with hearing loss. *Eur J Med Genet*. 2019;62:103724. doi: 10.1016/j.ejmg.2019.103724
61. Mauvais-Jarvis F. Sex differences in energy metabolism: natural selection, mechanisms and consequences. *Nat Rev Nephrol*. 2024;20:56–69. doi: 10.1038/s41581-023-00781-2
62. Koceva A, Herman R, Janez A, Rakusa M, Jensterle M. Sex- and gender-related differences in obesity: from pathophysiological mechanisms to clinical implications. *Int J Mol Sci*. 2024;25:7342. doi: 10.3390/ijms25137342
63. Cheng Y, Yuan Q, Vergnes L, Rong X, Youn JY, Li J, Yu Y, Liu W, Cai H, Lin JD, et al. KDM4B protects against obesity and metabolic dysfunction. *Proc Natl Acad Sci USA*. 2018;115:E5566–E5575. doi: 10.1073/pnas.1721814115
64. Félix-Soriano E, Sáinz N, Gil-Iturbe E, Collantes M, Fernández-Galilea M, Castilla-Madrigal R, Ly L, Dalli J, Moreno-Aliaga MJ. Changes in brown adipose tissue lipid mediator signatures with aging, obesity, and DHA supplementation in female mice. *FASEB J*. 2021;35:e21592. doi: 10.1096/fj.202002531R